



**THE EFFECT OF NANOPARTICLE  
ADDITIVES ON LITHIUM-ION MOBILITY  
IN A POLYMER ELECTROLYTE**

**HEIKI KASEMÄGI**

TARTU 2003

*Heiki Kasemagi Ph. D. Thesis*

**THE EFFECT OF NANOPARTICLE  
ADDITIVES ON LITHIUM-ION MOBILITY  
IN A POLYMER ELECTROLYTE**

**HEIKI KASEMÄGI**



TARTU UNIVERSITY  
PRESS

The study was carried out at the Institute of Materials Science of the University of Tartu.

The dissertation was admitted on May 8, 2003, in partial fulfilment of the requirements for the degree of Doctor of Philosophy in physics (solid state physics), and allowed for defence by the Council of the Department of Physics, University of Tartu.

Supervisors: Dr. Alvo Aabloo, Institute of Physics, Tartu University, Estonia

Prof. Josh Thomas, Department of Materials Chemistry,  
Uppsala University, Sweden

Opponents: Dr. Patrik Johansson, Condensed Matter Physics Group,  
Chalmers University of Technology, Gothenburg, Sweden

Prof. Peeter Burk, Institute of Chemical Physics,  
Tartu University, Estonia

Defence: On the 27<sup>th</sup> of June 2003 at the University of Tartu, Estonia

© Heiki Kasemägi, 2003

Tartu Ülikooli Kirjastus

[www.tyk.ut.ee](http://www.tyk.ut.ee)

Tellimus nr. 301

# Abstract

The rechargeable lithium-ion polymer battery has become a popular power source for many applications; typically, mobile phones, laptop computers and other small-size electronic equipment.

Poly(ethylene oxide) (PEO) is often seen as the prototype polymer electrolyte for modern battery concepts. Since PEO-based electrolytes are generally poor ion conductors at ambient temperatures due to their high degree of crystallinity, research focuses on the ways to improve their conductivities and mechanical properties at ambient and elevated temperatures.

Work over the last 20 years has shown that adding inorganic nanoparticles to a polymer/lithium-salt complex improves its ionic conductivity by an order of magnitude. This also increases the mechanical stability of the polymer host and the electrolyte-electrode interfacial stability.

Molecular Dynamics (MD) simulation is here used to study the structural and dynamical effects of adding  $\text{Al}_2\text{O}_3$ -nanoparticles to the  $\text{LiX}(\text{PEO})_n$  systems, where  $X = \text{Cl}, \text{Br}, \text{I}$  and  $\text{BF}_4$  and  $n = 10, 20, 35, 50$ . Simulation temperatures have been 290, 293, 330, 360 K.

Clear MD-simulation evidence for increased  $\text{Li}^+$  ion mobility is obtained on adding the nanoparticle into the PEO- $\text{LiBF}_4$  system. Ion-pairing/clustering effects and ion-mobility dependence on salt-type, concentration and temperature confirm earlier experimental observations. Changes are observed in the PEO/lithium-salt structure on adding the particle, especially the formation of an immobilised PEO “coordination sphere” around the particle; the influence of this on ion mobility is discussed.

# Contents

<b>Abstract</b>	<b>5</b>
<b>Contents</b>	<b>7</b>
<b>List of publications</b>	<b>9</b>
<b>List of Figures</b>	<b>10</b>
<b>1 Introduction</b>	<b>11</b>
1.1 The World's energy problem . . . . .	11
1.2 The Li-ion polymer battery . . . . .	12
1.3 An improved electrolyte . . . . .	13
1.4 Nanocomposite polymer electrolyte . . . . .	14
1.5 Aim of the Thesis . . . . .	17
<b>2 Molecular Dynamics (MD) simulation</b>	<b>19</b>
2.1 Computer-aided materials science . . . . .	19
2.2 The simulation method . . . . .	20
2.3 Potential Energy (PE) function . . . . .	22
<b>3 The simulated model</b>	<b>24</b>
3.1 The nanoparticle . . . . .	24
3.2 Details of the simulation . . . . .	24
<b>4 Results</b>	<b>29</b>
4.1 Effect of nanofiller on PEO structure and dynamics . . . . .	29
4.2 Effect of nanofiller on ion mobility . . . . .	31
4.3 Effect of nanofiller on salt aggregation . . . . .	33
<b>Concluding remarks</b>	<b>39</b>

<b>Future work</b>	<b>41</b>
<b>Kokkuvõte / Summary</b>	<b>42</b>
<b>Acknowledgements</b>	<b>44</b>
<b>References</b>	<b>46</b>
<b>PUBLICATIONS</b>	<b>53</b>

*Heiki Kasemagi Ph. D. Thesis*



# List of Publications

This Thesis comprises the present summary and the following publications, which are referred to in the text by their Roman numerals:

- I** “Molecular dynamics simulation of the effect of adding an Al<sub>2</sub>O<sub>3</sub> nanoparticle to PEO-LiCl/ LiBr/LiI systems”,  
**H. Kasemägi, M. Klintonberg, A. Aabloo and J. O. Thomas,**  
*J. Materials Chemistry*, 2001, **11**, 3191–3196.
- II** “Molecular dynamics simulation of the LiBF<sub>4</sub>-PEO system containing Al<sub>2</sub>O<sub>3</sub> nanoparticles”,  
**H. Kasemägi, M. Klintonberg, A. Aabloo and J. O. Thomas,**  
*Solid State Ionics*, 2002, **147**, 367–375.
- III** “MD simulation of temperature and concentration effects in the LiCl/PEO/Al<sub>2</sub>O<sub>3</sub> nanoparticle system”,  
**H. Kasemägi, M. Klintonberg, A. Aabloo and J. O. Thomas,**  
*Electrochimica Acta*, *In press*.

Papers of relevance to my work but not included in this Thesis:

- IV** “Molecular dynamics simulation of the effect of nanoparticle fillers on ion motion in a polymer host”  
**H. Kasemägi, M. Klintonberg, A. Aabloo and J. O. Thomas,**  
*Solid State Ionics*, *Accepted*.

# List of Figures

1.1	A PEO unit. . . . .	13
3.1	Crystal structure of a 14 Å diameter “spherical” corundum particle. . . . .	25
3.2	A 14 Å diameter “spherical” Al <sub>2</sub> O <sub>3</sub> particle after “computer annealing” at 2000 K. . . . .	25
3.3	A 14 Å diameter Al <sub>2</sub> O <sub>3</sub> particle in LiBF <sub>4</sub> (PEO) <sub>20</sub> before simulation. . . . .	25
3.4	A section of an amorphous PEO chain. . . . .	27
4.1	Atom density distribution for the 14 Å diameter Al <sub>2</sub> O <sub>3</sub> particle-LiCl(PEO) <sub>10</sub> system at 360 K. . . . .	30
4.2	A PEO chain around a 14 Å particle in LiBr(PEO) <sub>10</sub> at 360 K, showing the detailed structure around the Li <sup>+</sup> ion bound to the particle, and an example of an ion cluster. . . . .	30
4.3	Mean-square displacement (MSD) for Li <sup>+</sup> ion in LiBF <sub>4</sub> (PEO) <sub>20</sub> (particle-free) and in the LiBF <sub>4</sub> (PEO) <sub>20</sub> -14 Å diameter Al <sub>2</sub> O <sub>3</sub> particle system at 293 K. . . . .	32
4.4	Relative diffusion coefficients (D) for Li <sup>+</sup> ion in LiCl(PEO) <sub>x</sub> (particle-free) and > 4 Å from a 14 Å diameter Al <sub>2</sub> O <sub>3</sub> particle in LiCl(PEO) <sub>x</sub> ; x = 20, 35, and 50 . . . . .	33
4.5	Radial distribution function (RDF) and coordination number (CN) for Li-I for LiI(PEO) <sub>10</sub> and 14 and 18 Å diameter Al <sub>2</sub> O <sub>3</sub> particles in LiI(PEO) <sub>10</sub> at 360 K. . . . .	35
4.6	Radial distribution function (RFD) and coordination number (CN) for Li-B for LiBF <sub>4</sub> (PEO) <sub>20</sub> (particle-free) and the 14 Å diameter Al <sub>2</sub> O <sub>3</sub> particle in LiBF <sub>4</sub> (PEO) <sub>20</sub> at 293 K. . . . .	36

# Chapter 1

## Introduction

### 1.1 The World's energy problem

There is no doubts that one of the key challenges facing humanity is the energy problem: from where will our future energy come and where will we store it? There are two common types of energy source: fossil fuels and renewable energy sources. Until recently, fossil energy – energy from oil, gas, coal – corresponded to around 80 % of the World's energy supply. However, fossil-fuel resources are not endless; in fact, some will run out during the 21<sup>st</sup> Century. The burning of fossil fuel gives rise to global warming through the “green-house effect”. The goal to replace all fossil fuels by renewable energy sources – combustible renewables (biomass), waste, hydro-energy, wind energy, solar energy, geothermal energy – is a monumental challenge [1]. New problems arise like the too low efficiency of solar panels, wind- and wave-to-energy transformers, lack of hydro, wave and wind energy resources in some regions. Fuel cells as a means of energy conversion are also still in an early phase of development.

There is a one specific distinction between fossil-fuel and renewable energy sources: the renewable energy can be stored. Fossil fuels are natural energy stores before the energy is released, i.e., the fuel is burnt where needed and when needed. Most of the renewable energy sources (except biomass and hydro) lack such a feature. This is why the energy produced is usually transformed into electricity, which can then be readily transmitted over long distances and distributed to the consumers by power cables.

Since our means of storing electrical energy directly are limited, it must first be converted into some more convenient form: **potential, kinetic, thermal or chemical**. The focus of this Thesis is on chemical storage; namely, on secondary

(rechargeable) batteries in general, and the Lithium-Ion Polymer Battery (LIPB) in particular, as a device capable of electrical-to-chemical energy conversion and storage. The LIPB represent the present frontier in battery development.

## 1.2 The Li-ion polymer battery

The voltaic cell discovered in 1800 by Volta [2] is generally seen as the father (or perhaps the grandfather) of the modern battery. Interestingly, archaeologists believe [3] that a five-inch-long clay jar containing a copper cylinder encasing an iron rod, unearthed in 1938 in Khujut Rabu, outside Baghdad, Iraq, by the German archaeologist Wilhelm Konig was indeed the very first battery. Such a battery dates back to the period 250 BC to 225 AD – at least 1575 years before Volta's experiments!

The lithium-ion polymer battery (LIPB) is a rechargeable electrochemical device consisting of an anode and a cathode separated by solid polymer electrolyte containing a dissolved lithium salt to provide charge carriers. The most used cathode material today is  $\text{LiCoO}_2$  [4, 5]. However, recent studies focus on  $\text{LiFePO}_4$  [6] as a very promising cheaper cathode material. The anode consists typically of graphite;  $\text{LiBF}_4$  and  $\text{LiPF}_6$  are widely used lithium salts in the polymer electrolyte [7]. The electrolyte itself is usually a modification of poly(ethylene oxide) (PEO) (see below).

The advantages of an LIPB are:

- rechargeability – the same device can be used many times, typically  $> 1000$  charge-discharge cycles;
- it is a leak-proof system which is flexible under vibration and mechanical deformation;
- environmentally friendly - it contains no acids or heavy-metals;
- flexible and simple structure making possible the design of batteries in different shape;
- safety - no risk for explosion;
- it is already on the market – in laptops, mobile phones and other electronic equipment.

### 1.3 An improved electrolyte

Poly(ethylene oxide),  $(\text{CH}_2\text{-CH}_2\text{-O})_n$  [8], where the number of ethylene oxide (EO) units ( $n$ ) (Fig. 1.1) can be as many as one million, is probably the most studied host material for solid polymer electrolytes. The greatest strength of PEO is its ability to dissolve lithium salts and serve as an ion-conducting host. This was first noted for semi-crystalline PEO/alkali-salt complexes around 1973 [9, 10]. In 1978, the idea of a thin-film battery with a polymer electrolyte was presented. This marked the start of much research into solid polymer electrolytes for several electrochemical devices, including the rechargeable battery [11].

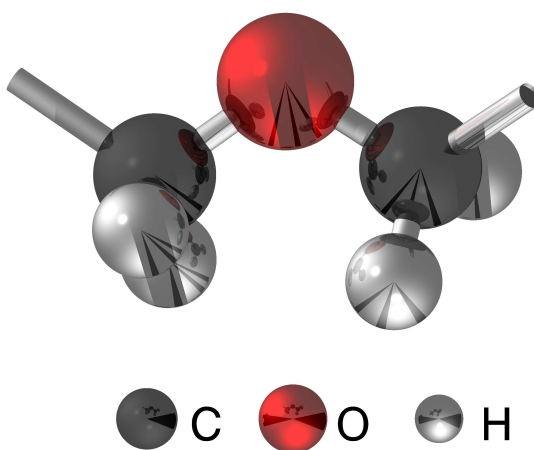


Figure 1.1: A PEO unit.

Polymer electrolytes, based on partially crystalline PEO and a high melting-point lithium salt, have good mechanical properties, but ion conductivities no better than  $10^{-8} \text{ S cm}^{-1}$  at room temperature; while a useful electrolyte for Li-ion battery applications should have a conductivity in the range  $10^{-2}$ - $10^{-3} \text{ S cm}^{-1}$  [7, 11]. The amorphous phase between crystalline regions is generally believed to be responsible of the ionic conductivity [12]. It was found that amorphous PEO and lithium-salt complexes can have conductivities upto  $10^{-5} \text{ S cm}^{-1}$  at 373 K, but at the expense of poorer mechanical properties [7].

The PEO chain provides coordination sites for Li ions, with typically 4-5 ether oxygens coordinating to each lithium [13]. The polarisability of the ether oxygens gives the ethylene groups an ability to dissolve a wide variety of salts [14]. The cation diffuses by changing its coordination sites along the chain by means of segmental motion, or by “hopping” between chains or between different parts of the same chain [7]. Anion diffusion is almost independent of the polymer chain.

There have been many attempts to increase the ionic conductivity and improve the mechanical properties of PEO as a host material, e.g., introducing new lithium-salt types or modifying PEO structure – different chain-lengths of PEO mixed together or combined with other polymer types to create disorder and thus reduce local crystallinity [15, 16]; segmented random or block copolymers or polymers with different side-chains (comb-branched copolymers) [17]; short PEO chains with reactive end-groups (methacrylate) forming cross-linked polymer networks with low or zero crystallinity at room temperature [18, 19]. Nevertheless, the highest conductivity achieved is still only about three orders of magnitude higher than that for partially crystalline PEO lithium-salt systems.

Another way to increase conductivity in polymer electrolytes without decreasing their mechanical properties is to introduce a “plasticizing agent” – small polar molecule – into the polymer matrix. This results in so-called *plasticized polymer electrolytes*, *polymer hybrids* and *gel electrolytes*. The ionic conductivity in such systems is close to that in liquid electrolytes. A number of polymer hosts (70–80 wt. %) in combination with different plasticising solvents (10–12 wt. %) have achieved the ionic conductivities in the range of  $10^{-4}$ - $10^{-3}$  S cm<sup>-1</sup> at room temperature [20].

PEO has been the polymer host most commonly “plasticized”. Quite good conductivities ( $10^{-3}$  S cm<sup>-1</sup>) were achieved at the expense of poor mechanical stability, mostly due to the increased solubility of the PEO in the solvent [21]. This can be reduced by cross-linking the polymers, which also helps to trap the liquid electrolyte inside the polymer matrix. Conductivities in the range of  $10^{-5}$ - $10^{-4}$  S cm<sup>-1</sup> and good mechanical properties were achieved at 293 K [22].

## 1.4 Nanocomposite polymer electrolyte

Incorporating nanoparticles into the polymer electrolyte is one way to “plasticize” the system. Nano-size particles are expected to decrease polymer crystallinity and increase the amorphous phase, thus increasing the ionic conductivity of the polymer, Li<sup>+</sup> ion transport number and the mechanical stability of the polymer host.

One of the first studies of a composite polymer was made in 1982 [23]. A study of  $\text{LiClO}_4(\text{PEO})_8$  containing  $\alpha\text{-Al}_2\text{O}_3$  powder showed that an inorganic filler greatly improves the mechanical stability of the polymer host; the optimal filler content was  $\approx 10$  vol. % within a limited temperature range; the  $\text{Li}^+$  transport number was  $\approx 0.25$  and was independent of temperature; however, the effect on ion conductivity was negligible.

A number of experimental studies have since shown evidence of enhanced ionic conductivity on adding an inorganic filler to a polymer-salt system. Some examples are presented in the Table 1.1. The filler types vary, including active, inert, conducting, organic and even ferroelectric particles:  $\alpha\text{-Al}_2\text{O}_3$  [23–25, 30],  $\gamma\text{-Al}_2\text{O}_3$  [28],  $\Theta\text{-Al}_2\text{O}_3$  [31],  $\text{TiO}_2$  [25, 32],  $\text{SiO}_2$  [26], NASICON [27], polyacrylamide (PAAM) [33],  $\text{BaTiO}_3$  [29, 34],  $\text{LiNbO}_3$  [29],  $\text{PbTiO}_3$  [29],  $\text{C}_{60}$  [35] etc.; filler-sizes cover the range from  $\mu\text{m}$ -size [29, 31, 34] down to nm-size [24–26, 28]. Different polymer hosts, like amorphous and crystalline PEO [23–29, 31, 33–35], oxymethylene linked PEO (OMPEO) [33], poly(ethylene glycol) (PEG) [30], 3PEG [32] with or without organic plasticizers such as dioctylphthalate (DOP), dibutylphthalate and dimethylphthalate [28] have also been used. The most popular lithium salts are  $\text{LiBF}_4$  [24] and  $\text{LiPF}_6$  [29] since these are favourable in commercial lithium-ion polymer batteries; also  $\text{LiI}$  [36],  $\text{LiClO}_4$  [23, 25, 28–30, 32, 34], lithium triflate ( $\text{LiCF}_3\text{SO}_3$ ) [29, 35], lithium TFSI ( $\text{LiN}(\text{CF}_3\text{SO}_2)_2$ ) [26, 29, 32], as well as salts containing other cations, like  $\text{NaI}$  [27, 31, 33], have also been studied.

One of the classical studies by Croce *et al.* [25] shows clear conductivity enhancement in the nanocomposite polymer electrolyte in the temperature range 303–353 K using  $\text{TiO}_2$  and  $\text{Al}_2\text{O}_3$ . They also show stable conductivity in the amorphous nanocomposite electrolyte at room temperature during several days, and a  $\text{Li}^+$  transfer number as high as 0.6 in the temperature range of 318–363 K, compared to the normal range of 0.2–0.3 in polymer/lithium-salt complexes.

Earlier studies [31] with micrometer-size fillers have already indicated that the conductivity enhancement may depend on filler size, with a large effect for smaller particle sizes. Krawiec *et al.* [24] find clear ionic conductivity dependence on particle size and ceramic content in the system. The conductivity reaches a peak at 10 wt. % of the nanosized fillers; this is at least an order of magnitude higher than for micrometer-size particles.

The conductivity dependence on filler-content with a peak at 10 vol. % is also

Table 1.1: Nanocomposite polymer electrolytes

Polymer-salt system	Filler			$\sigma / S \text{ cm}^{-1}$	T /K	Ref.
	Type	Size /nm	Content			
LiClO <sub>4</sub> (PEO) <sub>8</sub>	$\alpha$ -Al <sub>2</sub> O <sub>3</sub>		10 vol. %	5.0x10 <sup>-4</sup>	373	[23]
LiBF <sub>4</sub> (PEO) <sub>8</sub>	Al <sub>2</sub> O <sub>3</sub>	13	10 wt. %	5.0x10 <sup>-4</sup>	303	[24]
LiClO <sub>4</sub> (PEO) <sub>8</sub>	$\alpha$ -Al <sub>2</sub> O <sub>3</sub> , TiO <sub>2</sub>	6–13	10 wt. %	10 <sup>-5</sup> –10 <sup>-3</sup>	303–353	[25]
LiN(CF <sub>3</sub> SO <sub>2</sub> ) <sub>2</sub> (PEO) <sub>8</sub>	SiO <sub>2</sub>	7	13 wt. %	6.9x10 <sup>-5</sup>	373	[26]
NaI(PEO) <sub>10</sub>	NASICON			1.1x10 <sup>-5</sup>	303	[27]
LiClO <sub>4</sub> (PEO) <sub>8</sub> :DOP	$\gamma$ -Al <sub>2</sub> O <sub>3</sub>	10	10 wt. %	4.3x10 <sup>-4</sup>	302	[28]
LiClO <sub>4</sub> (PEO) <sub>8</sub>	BaTiO <sub>3</sub>	600–1200	1.4 wt. %	1.2x10 <sup>-3</sup>	343	[29]



shown by Przyłuski *et al.* [33]. Capiglia *et al.* [26] found that the conductivity is dependent on filler content, with a maximum at 13 wt. % in the case of SiO<sub>2</sub> at 373 K. The conductivity maximum is found to occur at a filler concentration of between 10 and 20 wt. % even for micrometer-size fillers [31].

Conducting NASICON was used as filler in the NaI-PEO complex in one of the earlier studies by Płocharski *et al.* [27]. The conductivity enhancement is believed to occur by increasing the proportion of amorphous phase.

Organic C<sub>60</sub> is also believed to work well as a structure-breaking plasticizer in the PEO-LiCF<sub>3</sub>SO<sub>3</sub> complex [35]. Raman studies show that it stabilises the polymer/salt structure at high temperatures, but otherwise has the rôle of an inert filler.

It is suggested that the increase in ionic conductivity for the PEG- $\alpha$ -Al<sub>2</sub>O<sub>3</sub>-LiClO<sub>4</sub> system [30] results from the interaction of the particle-surface acidic groups with anions and polyether oxygens, leading to a lowering of the transient cross-link density and a weakening of ion-ion interactions over the salt concentration range, where the increase in conductivity and decrease in viscosity are observed.

Ferroelectric materials (BaTiO<sub>3</sub>, LiNbO<sub>3</sub> and PbTiO<sub>3</sub>) as micrometer-size fillers in polymer-salt systems have also increase the ionic conductivity. It is suggested that the spontaneous polarisation of the ferroelectric material facilitates salt dissociation into charged fragments and produces a higher volume for the amorphous phase [29, 34].

Interfacial and mechanical stability is found to increase on adding fillers in a number of studies. Krawiec *et al.* report a factor two improvement in interfacial stability on the addition of Al<sub>2</sub>O<sub>3</sub>. The addition of BaTiO<sub>3</sub> assures interfacial stability [29, 34]. NMR and X-Ray studies show the stability of the amorphous structure at room temperature [31].

Several studies have shown higher Li<sup>+</sup> transport number compared to the same polymer/salt system without nanoparticles. As well as the 0.6 of Croce *et al.* [25], Capiglia *et al.* [26] reach the number 0.19 at 13 wt. % SiO<sub>2</sub> filler at 373 K; Sun *et al.* [29, 34] 0.37 at 343 K, and 0.52 at 358 K.

## 1.5 Aim of the Thesis

The main aim of this Thesis is to provide some deeper insights into the structure and dynamics of nanocomposite polymer electrolytes for lithium-ion polymer bat-

tery applications. This is achieved by performing Molecular Dynamics (MD) simulations of models representing the structure of the nanocomposite polymer electrolyte, consisting of amorphous poly(ethylene oxide) (PEO) as a host material complexed with various lithium salts and an inorganic filler. MD is a remarkable tool which can extend our knowledge and understanding of materials and their properties for situations where common experimental methods are less effective or even unrealistic. The problems to be studied are:

- The effect of an  $\text{Al}_2\text{O}_3$  nanofiller on PEO structure and dynamics:
  - with different lithium salts: LiCl, LiBr, LiI and  $\text{LiBF}_4$
  - at different salt concentrations (Li:EO ratio): 1:10, 1:20, 1:35 and 1:50
  - at different simulation temperatures: 290, 293, 310, 330 and 360 K
- The effect of the nanofiller on salt aggregation at different salt concentrations and at the simulation temperatures stated above.

## Chapter 2

# Molecular Dynamics (MD) simulation

### 2.1 Computer-aided materials science

Molecular Dynamics (MD), Molecular Mechanics (MM), Monte Carlo (MC) simulations and Quantum Chemistry (QC) calculations are all the tools of computer-aided materials science. Although the precise terminology varies, the principle is simply that we use computation in support of experimental materials science [37]. In fact, both move along together: computer calculations can help to prepare experiments and predict results. On the other hand – they can help explain experimental results. The computer is often also needed to extract ‘humanly readable’ data from a complex calculations; we call this “analysis”.

Computer-aided materials science involves not only calculations; visualisation also has a very important rôle in understanding materials and bringing a mathematical representation “to life”. Crystallographers often plot structures that result from diffraction data. Such models can be rotated and manipulated in space; structural differences between similar structures can be compared and visualised. There are a number of other ways to use visualisation as a valuable tool in materials research.

Computers can also help us to design new materials, or study the properties of materials yet unexplored experimentally. In computer calculations, it is also common that the complexity of the system must be reduced or simpler subsystems created. These must be simple enough to be represented by viable models, so that analytical and/or numerical methods can be used to analyze the system and its behaviour.

## 2.2 The simulation method

Molecular Dynamics (MD) simulation [38–41] is one way to perform ‘computer experiments’. In reality, atoms, ions and molecules are not static. MD allows us to simulate the dynamics of the particles and give us deeper insights into the local structure and into the changes in structure with time. Motion is inherent to all chemical processes; simple vibrations, like bond-stretching and angle-bending, can be registered by infrared (IR) spectra. Chemical reactions, hormone-receptor binding, and other complex processes are associated with many kinds of inter- and intramolecular motion.

According to statistical physics, physical quantities are represented by averages over configurations distributed according to a certain statistical ensemble. Since MD is a statistical mechanics method, and a trajectory in the  $6N$ -dimensional phase space obtained by MD provides such a set of configurations, a measurement of a physical quantity by simulation involves an arithmetic averaging of the various instantaneous values assumed by that quantity during the simulation. The most used ensembles in MD correspond to different experimental conditions like:

- A canonical ensemble (NVT); where the number of atoms (ions)  $N$ , volume  $V$  and temperature  $T$  are kept constant.
- A microcanonical ensemble (NVE); a constant system energy.
- An isothermal-isobaric ensemble ( $NpT$ ); where the system pressure  $p$  is constant.

In this way, statistical mechanics links microscopic behaviour with thermodynamics, thus making MD simulation a good tool to measure thermodynamic properties.

In short, classical MD can be defined as *a computer simulation technique where the time evolution of a set of interacting atoms (and/or ions) in an appropriately chosen simulation box is followed by integrating their Newton’s equations of motion*. It is clear that this definition is somewhat formal and needs some explanation.

In MD, Newton’s equation of motion;

$$\mathbf{F}_i = m_i \mathbf{a}_i \quad (2.1)$$

is applied for each atom  $i$  in the system of  $N$  atoms. Here,  $m_i$  is the atom mass,  $\mathbf{a}_i = d^2\mathbf{r}_i/dt^2$  its acceleration, and  $\mathbf{F}_i$  the force acting upon it due to its interactions with other atoms. The atoms are assigned initial velocities that conform

to the total kinetic energy of the system which, in turn, is dictated by the desired simulation temperature. This is achieved by slow “heating” of the system (usually starting at 0 K in an NVE ensemble) and then equilibrating the system at a desired temperature (often as an NVT ensemble). The simulation then follows, and the choice of ensemble depends on the problem in hand. Under normal conditions, it would be NpT.

The basic steps of the MD simulation are the simultaneous calculations of the force on each atom and, from this, the determination of the position of each atom over a specific period of the time. The force on an atom can be calculated as the derivative of the energy with respect to the change in atom-position:

$$\frac{-dE}{d\mathbf{r}_i} = \mathbf{F}_i = m_i \frac{d^2\mathbf{r}_i}{dt^2} \quad (2.2)$$

The position for each atom over a series of very small time-steps can be calculated knowing the atomic forces and masses. The resulting series of snapshots of structural changes over time is a trajectory. This is not obtained directly from Newton’s equations of motion due to the lack of an analytical solution. Instead, a number of numerical methods are used. The most common is probably the ‘leapfrog’ algorithm, where:

1. The acceleration  $\mathbf{a}_i$  at time  $t$  is calculated according to (2.2).
2. The velocity  $\mathbf{v}_i$  is updated at  $t + \Delta t/2$  as:

$$\mathbf{v}_i(t + \Delta t/2) = \mathbf{v}_i(t - \Delta t/2) + \mathbf{a}_i(t)\Delta t \quad (2.3)$$

where  $\Delta t$  is the time-step between two following states.

3. The atom position  $\mathbf{r}_i$  at  $t + \Delta t$  is updated as:

$$\mathbf{r}_i(t + \Delta t) = \mathbf{r}_i(t) + \mathbf{v}_i(t + \Delta t/2)\Delta t \quad (2.4)$$

Usually, the choice of method depends on the problem in hand. Classical MD allows us to simulate systems containing 1000–100000 atoms. The time-step is of order of 1 femtosecond; the simulation time is upto 1 microsecond. The appropriate system-size and simulation-time depends on the computing power and time available.

MD simulation is based on some approximation: first, the Born-Oppenheimer approximation is applied – where the system’s wavefunction consists of two separate parts: the wavefunction for electrons and the wavefunction for nuclei. This

can be done because of the mass of the nuclei is much greater than that of the electrons. The electronic Schrödinger equation can then be solved for each set of nuclear position to get the energy contributed by the electrons. This energy, along with nuclear-nuclear repulsion, then determines the total potential energy and can be used to find the forces on the atoms. The electronic energy and forces can be calculated once for a set of nuclear coordinates, and the forces and energies extrapolated between these coordinates. This energy (now a function of atomic position only) is called the *potential energy surface*.

The nuclei are then treated as classical particles moving on the potential energy surface, and the Schrödinger equation is replaced by Newton's equations of motion (2.2). This is the second approximation.

Thirdly, the potential energy surface is approximated to by an analytic potential energy function which gives the potential energy and interatomic forces as a function of the coordinates.

Introducing these approximations, especially a classical force field, rises the question whether it is justified to move atoms as classical particles without applying quantum laws? A classical approach is clearly poor for very light systems like  $H_2$  and He. Also, quantum effects become important when the temperature becomes sufficiently low.

## 2.3 Potential Energy (PE) function

Results of an MD simulation depend largely on the interatomic forces, and the use of MD simulation depends on the availability of good interatomic potential energy functions [38, 41]. The three main ways to obtain interatomic forces are:

- analytic potentials based on *ad hoc* functional forms and assumptions;
- analytic potentials with forms derived from quantum-mechanical concepts;
- forces obtained directly from quantum-mechanical electronic structure calculations.

The first two methods fit the parameters of some type of function to a set of system properties like bond lengths, energies, vibrational frequencies for molecules; lattice constants, elastic moduli, solid defect energies. The third method does not need a functional form, but requires more computing resources and a choice of basis-set, etc.

To represent real system behaviour in a simulation, a potential function must have sufficient **accuracy** to reproduce interesting properties; **transferability** to be usable in situations for which the potential function was not fitted, since the calculation of forces is the most time consuming part of the simulation; and **computational efficiency**. Also, the nature of the potential function depends on the type of bonding being modelled: metallic, covalent, ionic, van der Waals, etc.

Heiki Kasemagi Ph. D. Thesis

## Chapter 3

# The simulated model

### 3.1 The nanoparticle

The nanoparticle was constructed from the crystal structure of  $\alpha$ -Al<sub>2</sub>O<sub>3</sub> (corundum). Corundum has a rhombohedral crystal structure with unit-cell parameters:  $a = 4.75 \text{ \AA}$  and  $c = 12.99 \text{ \AA}$  (hexagonal setting) [42] corresponding to the space group  $R\bar{3}c$  (No. 167) [43].

A neutral section of the corundum structure was extracted to be as spherical as possible. A smaller particle contained 23 Al<sub>2</sub>O<sub>3</sub> units (115 atoms) (Fig. 3.1), a larger one 67 units (335 atoms). The particles were then “computer-annealed” at 2000 K in vacuum to relax the particles.

Usually, relaxation occurs only for a certain depth from a material surface. Since the particles are nano-sized, relaxation influences the whole particle. As a result, the particle deforms a little, especially at the surface (see Fig. 3.2). The particle loses its symmetry, and ends up as a quasi-spherical particle. The corundum crystal structure is destroyed, and the oxygens tend to move to the surface. The average Al-O<sub>Al</sub> coordination number was 5, since Al is usually 4- or 6-coordinated.

### 3.2 Details of the simulation

The simulated models are summarised in the Table 3.1. The simulation-box sizes were chosen to leave the minimum distance between the particle surfaces in the periodic arrangement of particles the same as the particle diameter. The surface area of the 14 Å diameter particle is 300 m<sup>2</sup>/cc; for the 18 Å diameter particle 600 m<sup>2</sup>/cc. The 14 Å diameter particle occupies *ca.* 6 % of the total volume and



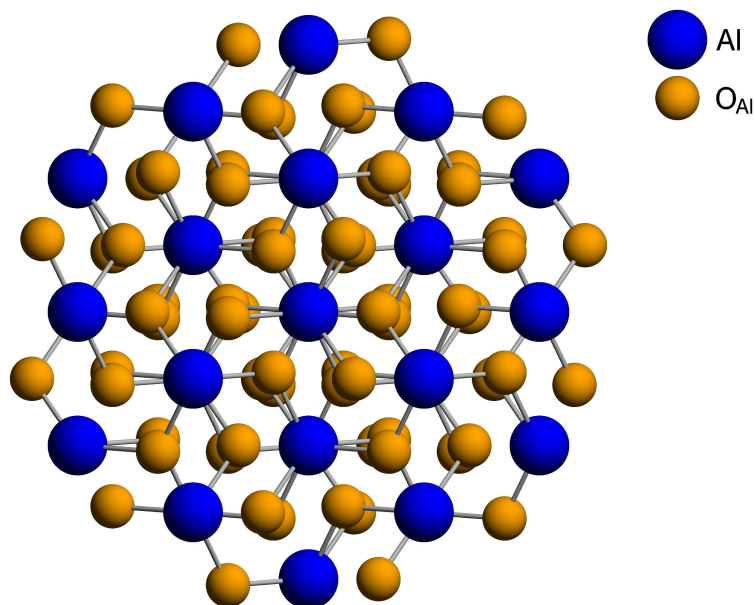


Figure 3.1: Crystal structure of a 14 Å diameter “spherical” corundum particle.

10 % of total mass; this is 10 % and 16 %, respectively, for the case of the 18 Å diameter particle.

For lithium tetrafluoroborate ( $\text{LiBF}_4$ ) in C models, the tetrafluoroborate ion ( $\text{BF}_4^-$ ) was treated as rigid ion, with B-F distances 1.39 Å and F-F distances 2.27 Å [44].

The first step to construct a simulation box was to place the “computer annealed” nanoparticle in the middle of the box. Salt ions were then inserted randomly around the particle. The last step was to fill the simulation box with an amorphous PEO chain by pivotal Monte-Carlo simulation [45] around the particle and salt ions (Fig. 3.3). In a model with no particle, only salt ions were inserted randomly into the simulation box and the amorphous PEO chain was then generated around the salt ions. In models with no particle or salt, the simulation box was only filled with an amorphous PEO chain (Fig 3.4).

MD simulations were performed with a local version of DL\_POLY [46]. The long-range interaction potential  $U(r)$  was described by the expression

$$U(r) = A \exp\left(-\frac{B}{r}\right) - \frac{C}{r^6} - \frac{D}{r^4} + \frac{q_1 q_2}{4\pi\epsilon_0 r} \quad (3.1)$$

A, B, C and D are potential parameters listed in Tables in papers **I**, **II** and **III**;  $r$  is the distance between atoms/ions participating in the interaction (in Å);  $q_i$  is the charge of an atom/ion participating in the interaction; electric constant  $\epsilon_0 = 8.854 \times 10^{-12}$  F/m. The potential parameters were developed earlier for PEO [47],  $\beta''$ -alumina [48], LiBr and Br-PEO [49, 50], LiCl, LiI, Li-PEO, Cl-PEO and I-PEO [51], LiBF<sub>4</sub> [44].

The simulations use periodic boundary conditions and an Ewald summation to calculate the electrostatic forces at longer distances. Each simulation consists of equilibrium period of 50 ps, followed by NVT (constant volume and temperature) simulation for 100 ps, and then NpT (constant pressure and temperature) simulation (Nosé-Hoover model) for upto 1000 ps. Sampling was made every 1 ps (every 1000 time-steps) during the NpT simulation. The models were prepared on local PC's and the final simulations made using the resources of the Parallel Computer Centre (PDC) of the Royal Institute of Technology (KTH) in Stockholm, the High Performance Computing Centre North (HPC2N), and our local PC-Wulfkit cluster of 4 Pentium III double-processor nodes.

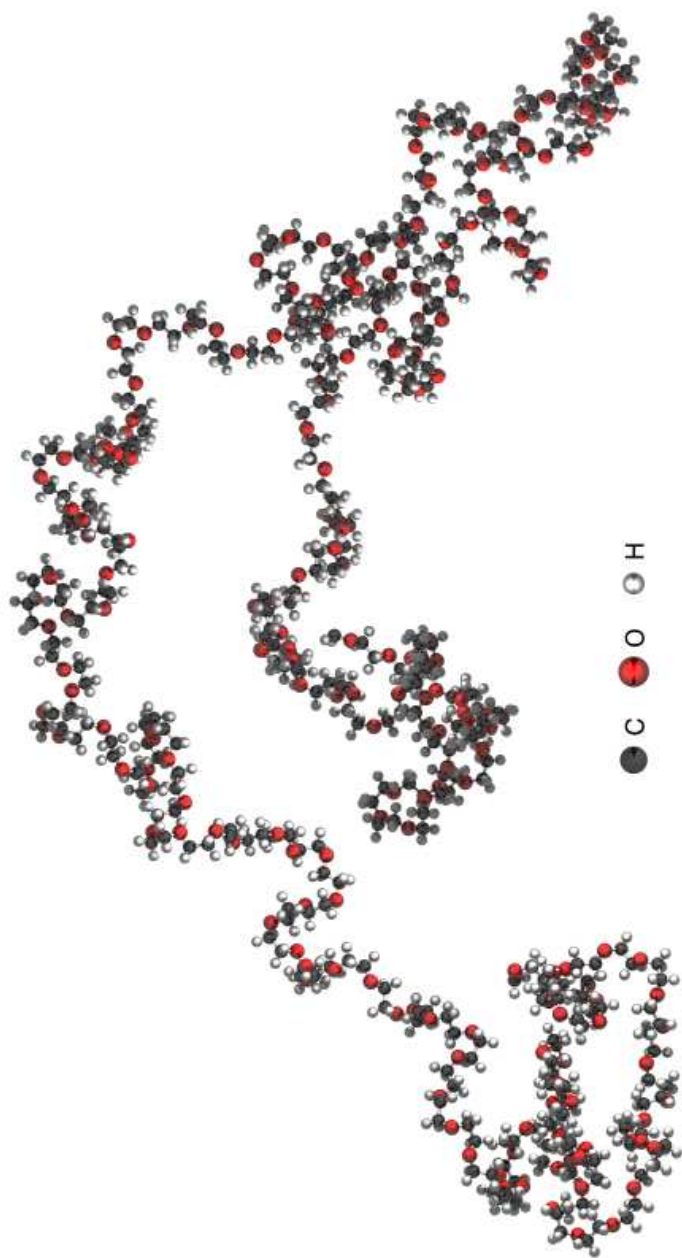


Figure 3.4: A section of an amorphous PEO chain.

Table 3.1: Simulated models

Type	Simulation box /ÅxÅxÅ	EO	Salt	Li:EO diameter /Å	Particle	Temp. /K
A01	26x21x22	200	–	–	–	360
A02	26x21x22	200	LiCl	1:10	–	360
A03	26x21x22	200	LiBr	1:10	–	360
A04	26x21x22	200	LiI	1:10	–	360
A05	31x31x31	455	–	–	14	360
A06	31x31x31	455	–	–	14	360
A07	31x31x31	455	–	–	14	360
A08	31x31x31	455	LiCl	1:10	14	360
A09	31x31x31	455	LiBr	1:10	14	360
A10	31x31x31	455	LiI	1:10	14	360
A11	37x37x37	787	–	–	18	360
A12	37x37x37	787	–	–	18	360
A13	37x37x37	787	–	–	18	360
A14	37x37x37	787	LiCl	1:10	18	360
A15	37x37x37	787	LiBr	1:10	18	360
A16	37x37x37	787	LiI	1:10	18	360
B01	24x24x24	200	LiBF <sub>4</sub>	1:20	–	293
B02	31x31x31	455	LiBF <sub>4</sub>	1:20	14	293
B03	14x14x200	294	LiBF <sub>4</sub>	1:20	slab	293
C01	28x22x24	200	LiCl	1:20	–	290, 330
C02	28x22x24	200	LiCl	1:35	–	290, 330
C03	28x22x24	200	LiCl	1:50	–	290, 330
C04	33x33x33	455	LiCl	1:20	14	290, 330
C05	33x33x33	455	LiCl	1:35	14	290, 330
C06	33x33x33	455	LiCl	1:50	14	290, 330

# Chapter 4

## Results

### 4.1 Effect of nanofiller on PEO structure and dynamics

The nanoparticle has a clear effect on the structure of the PEO host. It appears that the concentration of ether-oxygens ( $O_{et}$ 's) increases in the region *ca.* 3–4 Å from the particle surface (Fig. 4.1). This can be seen as the formation of a PEO “coordination sphere” around the nanoparticle. This forms for both particle sizes, and the process is independent of temperature, salt-type and concentration – it is even independent of the presence of a salt. This is not a result of the polymer simply being forced away from the particle surface; on the contrary, the polymer was generated so as to fill the space left in the simulation box around the particle. Within the “coordination sphere”, a continuous section of PEO does not curl itself around the particle, but rather that the same chain approaches and leaves the particle at several points along its length (see Fig. 4.3), with upto 5 successive  $O_{et}$ 's in close proximity to the particle.

Wieczorek and co-workers have applied the *effective medium theory* to explain the higher conductivity on adding nanofillers to the polymer/salt system [33, 52]. According to this theory, the dispersed insulating particles are covered by a highly conductive interface layer on the surface of the particle additive.

Almost all the space around the nanoparticle and its PEO “coordination sphere” in the simulation box can be considered as a conductive interface due to the periodic boundary conditions applied to the simulation box during the simulation. The particles are close enough in the periodic arrangement that there are no polymer-salt regions not affected by the nanoparticle. The PEO “coordination sphere” serves as a contact layer between the particle surface and the highly conductive polymer regions.

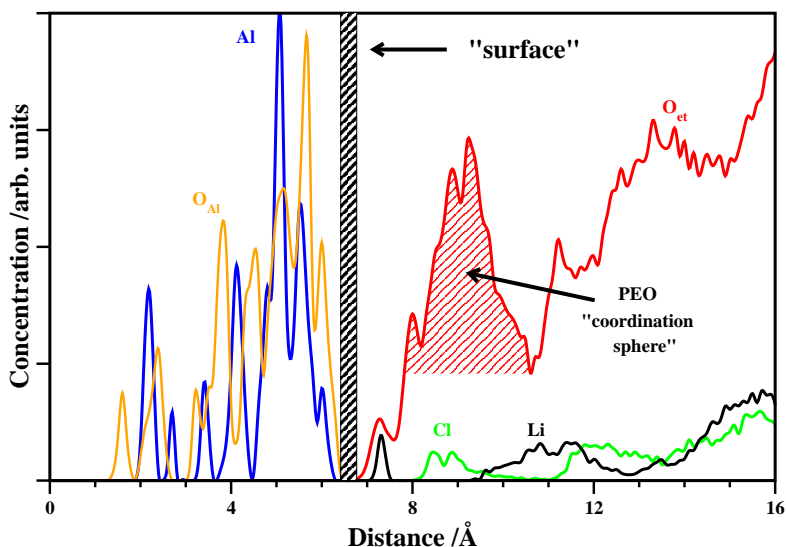


Figure 4.1: Atom density distribution for the 14 Å diameter  $\text{Al}_2\text{O}_3$  particle- $\text{LiCl}(\text{PEO})_{10}$  system at 360 K.

The PEO “coordination sphere” influences lithium-salt dissociation. Simulation results show that, for the lithium salts with monoatomic anion, some lithium ions are bound to the particle surface covered by polymer chain (Fig. 4.3). This means that less lithium ions occur in the regions away from the particle surface. This effect appears at all concentrations and temperatures. From simulations with  $\text{LiCl}$  at lower temperatures and concentrations, it appears that some  $\text{Cl}^-$  ions and even  $\text{Li}^+-\text{Cl}^-$  ion-pairs can also be located in the region of the PEO “coordination sphere”.

In the case of the lithium salt with a polyatomic anion ( $\text{BF}_4^-$ ), the anions are found between the particle surface and “coordination sphere”. This effect should leave more lithium ions in the region away from the particle surface than anions. The particle along with the “coordination sphere” thus helps the polymer to disassociate the salt-ions.

The formation of the PEO “coordination sphere” around the nanoparticle can

be explained by Lewis acid-base reactions involving a filler, polymer and salt ions [30, 53–55].  $\alpha$ -Alumina has Lewis-acid centres on the surface Al atoms and Lewis-base centres on the surface-O atoms. The competition between the Lewis-base ether-O's in the polymer chain and the filler Lewis-base centres in the complexing of alkali metal cations (for example,  $\text{Li}^+$ ) is suggested to lead to the formation of different types of complexes, and thus to modification to the polymer structure. Although the simulated nanoparticle has only Al and O atoms on the surface, with no other surface groups like -OH, a similar process is also assumed to take place during the simulation. The acidic centres of alumina win the competition with the Lewis-acid alkali metal cations in the formation of complexes with the polymer chain. Some salt ions also win to form complexes with filler.

A nanofiller certainly has an effect on PEO chain dynamics. At all temperatures and in all simulated models with a nanoparticle, the PEO chain mobility decreases dramatically in the region of the PEO “coordination” sphere. This is certainly an artifact of the particle-chain interaction. The part of the chain forming the “coordination sphere” is bound to the particle; this makes it immobile. The chain mobility is higher in regions away from the immobilised “coordination sphere” but still lower than in models without a particle. Interestingly, the chain is seen to be more mobile both near and away from the 18 Å diameter particle than for the 14 Å diameter particle. This could well be an unfortunate artifact of the arbitrary condition that the distance between the particles is equal to the particle diameter, since there is more “bulk” PEO in the 18 Å diameter particle case. For  $\text{LiBF}_4$ , the ether-O mobility increases slightly more than in the particle-free system; it is still quite low in the “coordination sphere” region.

## 4.2 Effect of nanofiller on ion mobility

Since the polymer structure with and without salt changes on adding the nanoparticle, the salt-ion mobility also changes. Common to all salt types, temperatures and concentrations, the  $\text{Li}^+$  ion mobility is an order of magnitude smaller in the region of the immobilised PEO “coordination sphere”. This is reasonable considering the salt concentration is low in this region and some of these ions or ion-pairs are bound to the particle. Since  $\text{Li}^+$  ion diffusion mechanism in the polymer host must be closely related to the dynamics of the polymer chain, then low mobility of the “coordination sphere” is another factor which reduces the  $\text{Li}^+$  ion mobility. At the same time,  $\text{Li}^+$  mobility is relatively high in regions away from the particle surface, where the polymer chain is much more mobile and the salt concentration higher.

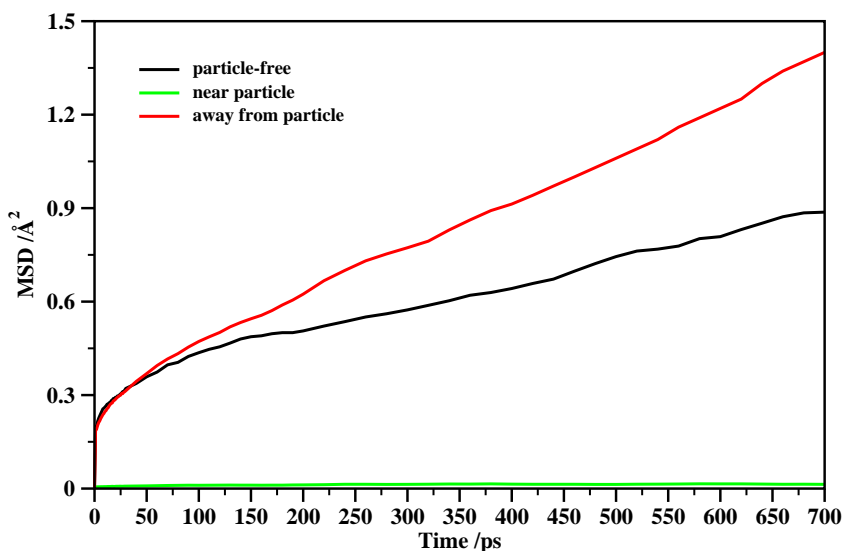


Figure 4.3: Mean-square displacement (MSD) for  $\text{Li}^+$  ion in  $\text{LiBF}_4(\text{PEO})_{20}$  (particle-free) and in the  $\text{LiBF}_4(\text{PEO})_{20}$ -14 Å diameter  $\text{Al}_2\text{O}_3$  particle system at 293 K.

The nanoparticle was expected to increase  $\text{Li}^+$  ion mobility in the regions away from the particle surface compared to the particle-free models. This effect appeared clearly on adding the particle into the  $\text{LiBF}_4$ -PEO system; the  $\text{Li}^+$  ion mobility almost doubles (see Fig. 4.3)

The temperature and concentration dependence study for  $\text{LiCl}$  shows the same general trends for  $\text{Li}^+$  ion mobility in regions away from the particle surface as those in a particle-free system. The most noticeable overall effect is that, at all temperatures, the  $\text{Li}^+$  ion mobility passes through a minimum at intermediate concentration ( $n = 35$ ) (Fig. 4.4). Also, the mobilities are slightly higher (not more than 25 %) in regions away from the particle surface than in the particle-free system. This agrees with experimental results for the  $\text{LiPF}_6$ -PEO system [56], where PEO conductivity peaks at a Li:EO ratio of 1:30, passes a minimum on lowering the concentration, and decreases again after  $n \geq 100$ .

It is seen that higher concentrations do not increase the  $\text{Li}^+$  ion mobility away



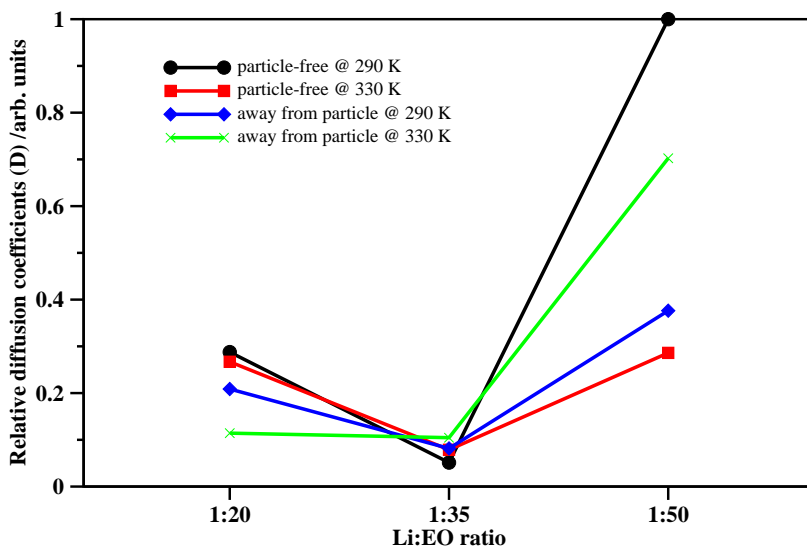


Figure 4.4: Relative diffusion coefficients ( $D$ ) for  $\text{Li}^+$  ion in  $\text{LiCl}(\text{PEO})_x$  (particle-free) and  $> 4 \text{ \AA}$  from a  $14 \text{ \AA}$  diameter  $\text{Al}_2\text{O}_3$  particle in  $\text{LiCl}(\text{PEO})_x$ ;  $x = 20, 35,$  and  $50$

from the particle surface, independent of temperature. However, a low concentration (1:50) at 330 K gives a clear increase in mobility away from the particle surface; only 40 % of this mobility is found in the particle free system; the opposite effect appears at 290 K.

$\text{Li}^+$  ion conductivity normally increases when temperature increases. However, simulation shows lower mobility at higher temperature. It is found experimentally [57] that, at least for the highly concentrated (1:4.5)  $\text{LiCl}$ -PEO system, the conductivity has a minimum around 333 K.

### 4.3 Effect of nanofiller on salt aggregation

Three parameters were used to characterise the “structure” in the analysis of simulation results:

- radial distribution function (RDF)

- coordination number (CN)
- number of “free”  $\text{Li}^+$  ions

The first RDF peak can usually indicate the general correctness of a simulation. It can also validate the quality of the force field used. If the first RDF peak for two atom-types is at too short a distance, then the forces between these atoms are too attractive.

The RDF data shows that the distances between Li and anions are in the expected range – for example, 2.25 Å for Li-Cl, 2.50 Å for Li-Br, and 2.70 Å for Li-I at 360 K ( $n = 10$ ; see Fig. 4.5). The differences come from the different sizes of anions:  $\text{Cl}^-$  ion is the smallest and  $\text{I}^-$  the biggest. The value around 3 Å is also reasonable for Li-B distances considering the B-F distance is 1.39 Å. These values remain the same if the nanoparticle is added into the system, and independent on salt concentration and simulation temperature.

The integral of the RDF over distance is called the coordination number. It shows how many atoms of one atom-type coordinate to atoms of another type *versus* distance. This is also a valuable parameter to show the relationship between an atom and its neighbours.

The coordination-number data suggest a highly sensitive ion-clustering effect with respect to the presence of the nanoparticle, anion-type, simulation temperature and salt concentration. Coordination-number values 1.5 for LiCl, 2.4 for LiI and 2.7 for LiBr at 360 K without the particle show that, in pure PEO-salt systems, there is large ion-clustering for salts with larger anions and ion-pairing for LiCl. Signs of ion-pairing appear also in the  $\text{LiBF}_4$ -PEO system, where the Li-B coordination number is slightly below 1 (Fig. 4.6). It is worth mentioning that, since LiCl shows the lowest coordination number among of the three salts simulated with monoatomic anions, it was chosen for temperature and concentration effect studies; and it appears that the Li-Cl CN does not rise above 1.5 during those simulations.

The addition of a nanoparticle certainly has an effect on ion aggregation. The effect is greatest in the  $\text{LiBF}_4$ -PEO system, where CN decreases from 0.9 to 0.7 (Fig. 4.6). The CN also decreases slightly at 290 K and 330 K for LiCl at  $n = 35$ , and more at 330 K and  $n = 50$  (from 1.5 to 0.9). Other salt type, temperature and concentration combinations show increased coordination number on adding the nanoparticle.

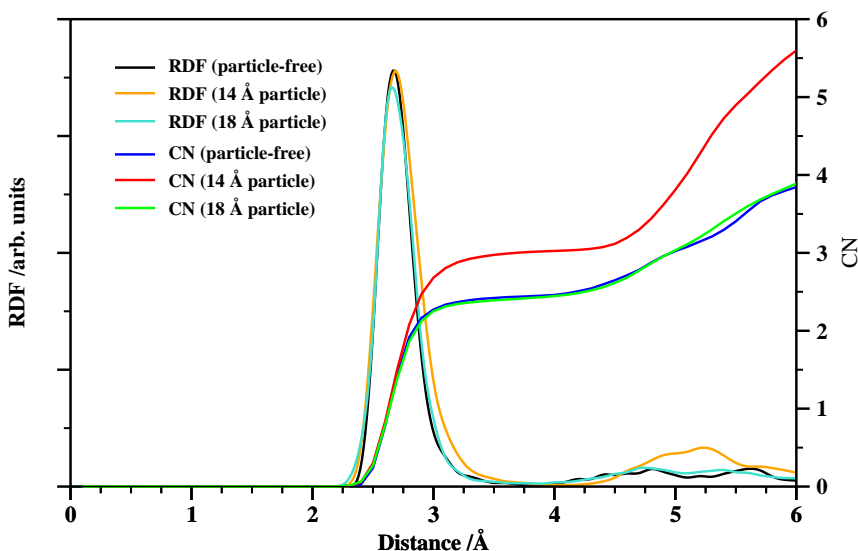


Figure 4.5: Radial distribution function (RDF) and coordination number (CN) for Li-I for LiI(PEO)<sub>10</sub> and 14 and 18 Å diameter Al<sub>2</sub>O<sub>3</sub> particles in LiI(PEO)<sub>10</sub> at 360 K.

The ion-aggregation effect can also be determined by counting “free” Li<sup>+</sup> ions; these are important as charge carriers. “Free” implies that these ions do not participate in ion-pairs and larger aggregates. Here, the best results again occur for the LiBF<sub>4</sub>-PEO system, where around 30 % of the Li<sup>+</sup> ions can be considered as “free”. Adding the nanoparticle into this system has a noticeable effect – increasing the ratio of “free” Li<sup>+</sup> ions to 40 %. Lithium salts with monoatomic anions show much poorer results. Very large salt clusters (10 and more ions) form at 360 K, especially in the case of LiBr and LiI; a tendency to form larger clusters on adding the nanoparticle can be noted. The cluster charges are not large though, as seen from the Fig. 11 in paper I. The number of “free” Li<sup>+</sup> ions in LiCl does not reach to the level shown for LiBF<sub>4</sub> as temperature and concentration changes. The higher concentration n = 20 shows a significant lack of “free” Li<sup>+</sup> ions. But it appears here that the addition of the nanoparticle increases the ratio of “free” Li<sup>+</sup> ions. The only case showing the opposite effect is n = 50 at 290 K.

A challenge facing polymer electrolytes is to dissociate the lithium salt and re-

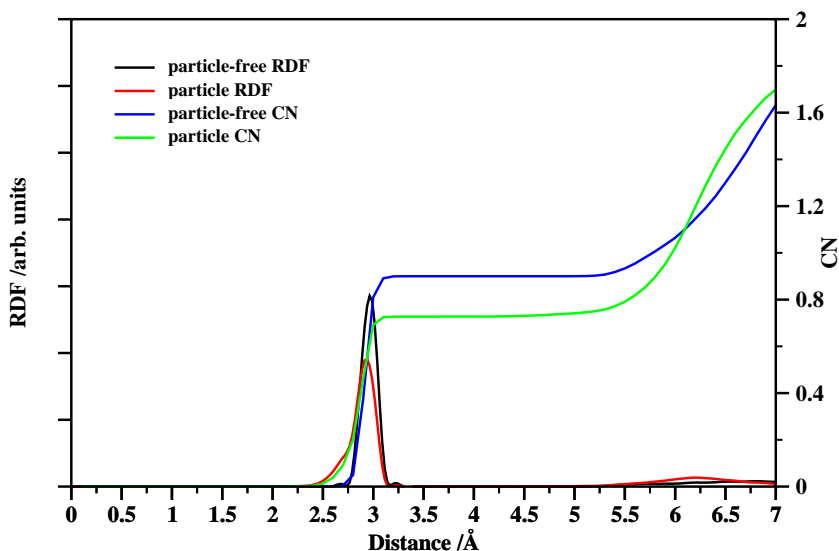


Figure 4.6: Radial distribution function (RDF) and coordination number (CN) for Li-B for  $\text{LiBF}_4(\text{PEO})_{20}$  (particle-free) and the 14 Å diameter  $\text{Al}_2\text{O}_3$  particle in  $\text{LiBF}_4(\text{PEO})_{20}$  at 293 K.

lease as many mobile lithium ions as possible. Salt crystallisation is common to organic (including biological) and inorganic systems; depending on the system, this may be a desired effect (we all make good use of our fingernails!). In the design of the lithium-ion polymer battery, much effort is made to dissolve the lithium salt as well as possible. The conductivity depends on the number of mobile “free” charge carriers. However, high salt concentrations can lead to the formation of ion-pairs and larger aggregates, resulting in decreased conductivity; also, the polymer chain becomes stiffer, leading to an additional lowering of the conductivity [58].

The salt-ion pairing/clustering effect has been studied previously both experimentally and theoretically by molecular dynamics simulation. Experimental results show that the ion-pairing depends on the salt concentration in  $\text{NaCF}_3\text{SO}_3\text{-PEO}$  complexes [59]. The fraction of “free” ions decreases with increasing salt concentration. This is believed to be a result of decreasing the distances between ions

with increasing salt concentration, until ion-ion interactions become significant. Also, the fraction of ions participating in ion-pair formations is seen to increase with temperature for these same complexes. This temperature dependence is explained [60] to be a result of entropy changes during salt dissociation-association. If salt dissociates in the polymer matrix at lower temperature, then the decrease in entropy is the result of restricted segmental and translational vibrational modes of the polymer. At higher temperatures the entropy increases again due to the ions associating less with the polymer and more with each other, possibly leading to an “out-salting” effect at high temperatures.

Molecular mechanics and dynamics studies of LiBr-PEO complexes [61] show Li-Br pairing to be likely even for an Li:EO ratio of 1:50. The concentration of Li-Br pairs is seen to increase with LiBr concentration in PEO. Also, more ion pairs are found to form at 400 K than at 300 K. In LiI-PEO, MD simulation [62] shows the fraction of “free” ions to decrease with increasing salt concentration. Large clusters become more important at higher salt concentrations, as also reported for amorphous PEO-NaI complexes [63].

Salt aggregation is the key to understanding why the  $\text{Li}^+$  ion mobility sometimes increases on adding the nanoparticle and sometimes decreases. Three variables play their rôle together: salt-type, salt-concentration and simulation temperature. On adding the nanoparticle into  $\text{LiBF}_4(\text{PEO})_{20}$  system at 293 K, the  $\text{Li}^+$  ion mobility increases. It appears that large polyatomic anions have some advantages over their mono-atomic counterparts in promoting lithium mobility: the salt dissolves better, even without the nanoparticle; adding the particle decreases the Li-B coordination number, indicating that there are potentially more mobile lithium ions in regions away from the particle surface. The anions bound to the particle surface leave potentially “free” mobile lithium ions away from the particle surface. Apparently, the chosen simulation temperature and salt concentration is a successful combination to give increased  $\text{Li}^+$  ion mobility on adding the nanoparticle.

Although lithium salts with mono-atomic anions have a greater tendency to cluster, it is still possible to enhance  $\text{Li}^+$  ion mobility on adding the nanoparticle by reducing the salt concentration and changing the temperature, as seen for LiCl. Adding the nanoparticle at  $n = 50$  and 330 K, the Li-Cl coordination number decreases and the number of free ions increases from 0 % to 11 %. All this leads to increased  $\text{Li}^+$  ion mobility. Here, low salt concentration can be seen as a key to mobility enhancement.

The opposite occurs at higher salt concentrations:  $n = 10$  is apparently too high a concentration for all simulated lithium salts with monoatomic anions. The LiCl example shows that even  $n = 20$  is too high a concentration; adding the nanoparticle increases the Li-Cl coordination number and consequently the ion-pairing. This is also reflected in the low ratio of “free”  $\text{Li}^+$  ions away from the particle surface.

Heiki Kasemagi Ph. D. Thesis

# Concluding remarks

This Thesis summarises the results of molecular dynamics studies of the effect of an inorganic nanofiller on polymer/lithium-salt complexes. The results are a good illustration of what can realistically be achieved through MD simulation. One must admit that real systems are much more complicated both from a particle as well from a polymer-salt complex viewpoint. The limiting factors of simulation of real systems are the lack of suitable force fields, the limited number of atoms in the simulation box, and the simulation time due to the availability of computational power and time. Nevertheless, some important features are seen relevant to lithium-ion polymer battery design:

- MD simulations show clear evidence of enhanced  $\text{Li}^+$  ion mobility away from the particle surface compared to that in a particle-free  $\text{LiBF}_4$ -PEO system.
- $\text{Li}^+$  ion mobility enhances at lower salt concentration on adding the nanoparticle in the regions away from the particle surface.
- Higher salt concentrations lead to a decreased fraction of “free”  $\text{Li}^+$  ions and the formation of larger clusters. Adding nanoparticles increases this effect and consequently decreases  $\text{Li}^+$  ion mobility away from the particle surface.
- Formation of an immobilised PEO “coordination sphere” around the nanoparticle is independent of salt-type, concentration and simulation temperature.
- $\text{Li}^+$  ions bind to the particle surface for  $\text{LiCl}$ ,  $\text{LiBr}$  and  $\text{LiI}$  salts at all temperatures and concentration, thus reducing the ratio of potentially mobile  $\text{Li}^+$  ions in regions away from the particle surface and thus also the mobility. Bound  $\text{Li}^+$  ions are immobile as is the polymer chain and thus do not contribute to the mobility.

- $\text{BF}_4^-$  ions bind to the particle surface, leaving potentially mobile “free”  $\text{Li}^+$  ions in regions away from the particle surface which can contribute to enhancing the  $\text{Li}^+$  ion mobility.

For a battery electrolyte, the salt-type must be chosen carefully. More attention must be paid to lithium salts with polyatomic anions like lithium triflate ( $\text{LiCF}_3\text{SO}_3$ ), lithium imide ( $\text{LiN}(\text{CF}_3\text{SO}_2)_2$ , LiTFSI),  $\text{LiPF}_6$ ,  $\text{LiBF}_4$ , etc. Salt concentration should be low enough to avoid the serious ion-pairing/clustering effects. These effects also depend strongly on temperature. The particle concentration can also be optimised – usually to around 10 wt. %.

Heiki Kasemagi Ph. D.



## Future work

The lithium-ion polymer battery is not immune to the growing importance of “Nanoscience”. Many studies have been made of  $\text{TiO}_2$  and  $\text{Al}_2\text{O}_3$  nanoparticles in different polymer-lithium salt systems in Monash University, Melbourne [64]. MD is an appropriate tool to expand our understanding of these experimental results. Research groups from Utah (USA) and Gothenburg (Sweden) [65] have already made some initial MD and quantum chemistry calculations of  $\text{TiO}_2$ /PEO/lithium-salt system.  $\text{TiO}_2$  is interesting because of its natural chemical activity. Nevertheless, passive  $\text{SiO}_2$  nanoparticles are also an interesting subject for simulation in the polymer electrolyte. Also, the simulation of organic  $\text{C}_{60}$  in the polymer/lithium-salt system [35] would be an interesting challenge.

MD simulations are also underway of novel crystalline PEO/lithium-salt systems. For at least the last 20 years, crystalline PEO/lithium-salt systems have shown orders of magnitude lower conductivity than their amorphous counterparts. Recently, however, a new crystalline PEO/lithium-salt system has shown higher conductivity than in its amorphous form [66–69]. MD simulations of this new crystalline system,  $\text{LiPF}_6(\text{PEO})_6$ , are underway and promise to give us valuable data about structural and dynamical aspects of this fundamental question. There are also interesting possibilities to study the effects of chain length and displacement on ion dynamics and local structure in this type of system.

An exciting vision is also to simulate a nano-system containing an effective cathode, anode and polymer electrolyte – indeed, a lithium-ion polymer “nano”-battery!

# Kokkuvõte / Summary

## Anorgaaniliste nanolisandite mõju liitiumiooni liikuvusele polümeerelektrolüüdis

Liitiumioon-polümeeraku on muutunud väga populaarseks ja laialt kasutatavaks energiaallikaks mitmekesistes portatiivsetes elektroonikaseadmetes nagu mobiiltelefonid, laptop- ja pihuarvutid jne.

Polüetüleenoksiid (PEO) on palju-uuritud materjal, mis on kaasaegse polümeeraku struktuuris saavutanud olulise tähtsuse kui elektrolüüdi prototüüp. Et PEO-l põhinevate elektrolüütide ioonjuhtivus on normaaltemperatuuril suhteliselt väike polümeeri kristalse faasi suure osakaalu tõttu ega ole piisav rahuldamiseks reaalsete rakenduste vajadusi, siis on uuringutes keskendutud antud elektrolüütide juhtivus- ja mehaaniliste omaduste parendamisele normaaltemperatuuril.

Viimase 20 aasta uuringute tulemused on näidanud, et anorgaaniliste nano-osakeste lisamine polümeerelektrolüüdi ja liitiumsoola kompleksi parandab elektrolüüdi ioonjuhtivust mitme suurusjärgu võrra. Samaaegselt paranevad ka selle mehaanilised omadused ning elektrolüüdi-elektroodi puutekihi stabiilsus.

Käesolevas töös kasutatakse molekulaardünaamilist (MD) simulatsiooni, et uurida struktuuri- ja dünaamika muutusi  $\text{Al}_2\text{O}_3$  nano-osakeste lisamisel  $\text{LiX}(\text{PEO})_n$  süsteemi. Liitiumsoola anioonideks (X) on  $\text{Cl}^-$ ,  $\text{Br}^-$ ,  $\text{I}^-$  ja  $\text{BF}_4^-$ ; soola kontsentratsioon (etüleenoksiidi monomeeride arv ühe liitiumiooni suhtes (n)) on 10, 20, 35 ja 50; simulatsioonid teostati temperatuuridel 290 K, 293 K, 330 K ja 360 K.

Töös arutletakse PEO/liitiumsoola struktuuri muutuste, eriti nano-osakese ümber moodustuva PEO-kihi tekkepõhjuste ja mõju üle ionide liikuvusele. Nano-osakeste lisamisel PEO- $\text{LiBF}_4$  süsteemi temperatuuril 293 K saavutatakse MD-simulatsioonis osakesest eemalejäävates piirkondades ligikaudu kaks suurem Li-iooni liikuvus võrreldes süsteemiga, kus osakene puudub.

Simulatsioonides leiab kinnitust varasematest katseandmetest teadaolev soola-ioonide paardumise ja klasterdumise sõltuvus soola tüübist (kasutatavast anioonist), soola kontsentratsioonist ja temperatuurist. Soola väiksema kontsentratsiooni korral on nanoosakese lisamisel liitiumiooni liikuvus osakesest kaugemal olevates piirkondades suurem osakeseta süsteemiga võrreldes. Soola suurem kontsentratsioon vähendab “vabade” liitiumioonide arvu ja suurendab soolaklastritesse hõlmatud ionide arvu. Nano-osakese lisamisel süsteemi suureneb selle efekti mõju ja väheneb seega täiendavalt liitiumiooni liikuvus.

Väheliikuv PEO-kiht moodustub nano-osakese ümber kõigi kasutatavate soolatiüüpide, kontsentratsioonide ja temperatuuride korral. See kiht hoiab enda sees olevad soolaioonid väheliikuvad ja lahutab need kihist väljaspoole jäävatest vastasmärgilistest ionidest. Mono-aatomilise aniooniga soola korral seob nanoosake koostöös ümbritseva PEO-kihiga endaga liitiumioone, vähendades potentsiaalselt liikuvate liitiumioonide arvu kihist väljaspool;  $\text{LiBF}_4$  korral seotakse nano-osakesega aga  $\text{BF}_4^-$ -anioon, mistõttu suureneb potentsiaalselt liikuvate “vabade” liitiumioonide arv väljaspool kihti. Seega on PEO-kihi mõju kahetine sõltuvalt kasutatavast liitiumsoolast.

# Acknowledgements

It has always been difficult for me to express my gratitude – I cannot find the right words. But I can try!

My greatest thanks are addressed to my supervisor Professor Josh Thomas. Your practical lessons in preparing papers for publication are priceless. You always have lots of ideas for ongoing research, as well as for future projects. Thank You for making it possible for me to participate in a most important conference in battery-related research, and for making the trip such a wonderful experience. Thank You for all those corrections to my manuscripts. It was sometimes difficult to find my original text under your red ink. Thank You too for giving me the chance to work together with the wonderful people of the Department of Materials Chemistry at the Ångström Laboratory in Uppsala. Thank You for Everything.

I hope that my second supervisor, Alvo Aabloo, is not too upset about not being thanked first; it is difficult to write in parallel, so I have used the reverse order of the author names on our papers. Thank You for being such a strong supervisor, for catching me at the right time, and applying ‘pressure’ when it was needed – laziness is a human weakness, especially in this human. Thank You for patiently explaining so many new things to me, and for correcting me when I followed the wrong path. Most importantly - Thank You for exposing me to this interesting and challenging World of computer modelling, and for all those long talks about Life, the Universe – and Computers!

I’d also like to thank Dr. Mattias Klintonberg, Daniel Brandell and all the people of the Department of Materials Chemistry at the Ångström Laboratory. Knowing you were there and willing to help gave me a great feeling of security.

I also thank Professor Krister Källström and The Kami Research Foundation (KFS) for their financial support during these 4 years, and the Nordic Energy Research (NEFP) for their stipendium. Their annual “ski”-meetings were a great

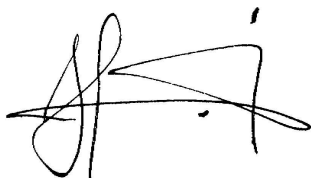
idea, giving us all an opportunity to meet new and interesting people, and to learn other research areas.

I'd like also to thank Professor Jaak Kikas and the Institute of Materials Science of the University of Tartu for all their support and help during my PhD studies.

Grants from the Swedish Research Council (VR), the Swedish Institute (SI) and the Estonian Science Foundation (ETF) are all gratefully acknowledged, as is the fine service provided by the High Performance Computing Centre North (HPC2N) and the Parallel Computer Centre (PDC) at KTH in Sweden.

Anti Liivat, Katrin Uba, Andi Hektor, Dr. Hugo Mändar, Dr. Alexandre Talyzine, Dr. Wiktor Tatara... – Thank You All for being great room-mates and for all the talks we have had.

To my Family – Thank You All for supporting me. It always gave me a warm feeling to get a phone-call from home during the long, cold winter nights in Uppsala. Finally, a special Thank You to my Dad for taking care of my house while I was away. Suut tänu teile kõigile!

A handwritten signature in black ink, appearing to be 'Heiki Kasemagi', written in a cursive style.

Tartu, April 2003

# References

- [1] R. M. Dell and D. A. J. Rand, “Energy storage — a key technology for global energy sustainability”, *J. Power Sources*, 2001, **100**, 2–17.
- [2] I. Buchmann, “Batteries in a portable world”, Cadex Electronics, *Second Ed.*, <http://www.buchmann.ca/>.
- [3] The Museum of Unnatural Mystery, <http://www.unmuseum.org/bbattery.htm>; BBC News, <http://news.bbc.co.uk/1/hi/sci/tech/2804257.stm>.
- [4] R. Koksang, J. Barker, H. Shi and M. Y. Saïdi, “Cathode materials for lithium rocking chair batteries”, *Solid State Ionics*, 1996, **84**, 1–21.
- [5] M. Winter, J. O. Besenhard, M. E. Spahr and P. Novák, “Insertion electrode materials for rechargeable lithium batteries”, *Advanced Materials*, 1998, **10**, 725–763.
- [6] A. S. Andersson, J. O. Thomas, B. Kalska and L. Häggström, “Thermal stability of LiFePO<sub>4</sub>-based cathodes”, *Electrochemical and Solid-State Letters*, 2000, **3**, 66–68.
- [7] F. M. Gray, “Polymer Electrolytes”, The Royal Society of Chemistry, Cambridge, 1997.
- [8] Y. Takahashi and H. Tadokoro, “Structural studies of polyethers,  $-(\text{CH}_2)_m\text{-O-})_n$ . X. Crystal structure of poly(ethylene oxide)”, *Macromolecules*, 1973, **6**, 672–675.
- [9] D. E. Fenton, J. M. Parker and P. V. Wright, *Polymer*, 1973, **14**, 589 in P. V Wright, “Polymer electrolytes — the early days”, *Electrochimica Acta*, 1998, **43**, 1137–1143.
- [10] P. V. Wright, *Br. Polymer J.*, 1975, **7**, 319 in P. V Wright, “Polymer electrolytes — the early days”, *Electrochimica Acta*, 1998, **43**, 1137–1143.

- [11] M. B. Armand, J. H. Chabagno and M. Duclot, *Second International Meeting on Solid Electrolytes*, St. Andrews, Scotland, 20-22 Sept. 1978 in M. Armand, "The history of polymer electrolytes", *Solid State Ionics*, 1994, **69**, 309–319.
- [12] C. Berthier, W. Gorecki, M. Minier, M. B. Armand, J. M. Chabagno and P. Rigaud, "Microscopic investigation of ionic conductivity in alkali metal salts-poly(ethylene oxide) adducts", *Solid State Ionics*, 1983, **11**, 91–95.
- [13] P. Lightfoot, M. A. Mehta and P. G. Bruce, "Crystal structure of the polymer electrolyte poly(ethylene oxide)<sub>3</sub>:LiCF<sub>3</sub>SO<sub>3</sub>", *Science*, 1993, **262**, 883–885.
- [14] D. Baril, C. Michot and M. Armand, "Electrochemistry of liquids vs. solids: polymer electrolytes", *Solid State Ionics*, 1997, **94**, 35–47.
- [15] R. Xue and C. A. Angell, "High ionic conductivity in PEO. PPO block polymer + salt solutions", *Solid State Ionics*, 1987, **25**, 223–230.
- [16] J. Przyłuski and W. Wiczorek, "Copolymer electrolytes", *Solid State Ionics*, 1992, **53-56**, 1071–1076.
- [17] F. M. Gray, J. R. MacCallum, C. A. Vincent and J. R. M. Giles, "Novel polymer electrolytes based on ABA block copolymers", *Macromolecules*, 1988, **21**, 392–397.
- [18] R. Huq, R. Koksang, P. E. Tonder and G. C. Farrington, "Effect of plasticizers on the properties of new ambient temperature polymer electrolyte", *Electrochimica Acta*, 1992, **37**, 1681–1684.
- [19] A. Reiche, A. Weinkauff, B. Sandner, F. Rittig and G. Fleischer, "Alternating copolymers for novel polymer electrolytes: the electrochemical properties", *Electrochimica Acta*, 2000, **45**, 1327–1334.
- [20] F. B. Dias, L. Plomp and J. B. J. Veldhuis, "Trends in polymer electrolytes for secondary lithium batteries", *J. Power Sources*, 2000, **88**, 169–191.
- [21] S. Chintapalli and R. Frech, "Effect of plasticizers on high molecular weight PEO-LiCF<sub>3</sub>SO<sub>3</sub> complexes", *Solid State Ionics*, 1996, **86-88**, 341–346.
- [22] M. C. Borghini, M. Mastragostino and A. Zanelli, "Reliability of lithium batteries with crosslinked polymer electrolytes", *Electrochimica Acta*, 1996, **41**, 2369–2373.

- [23] J. E. Weston and B. C. H. Steele, "Effects of inert fillers on the mechanical and electrochemical properties of lithium salt-poly(ethylene oxide) polymer electrolytes", *Solid State Ionics*, 1982, **7**, 75–79.
- [24] W. Krawiec, L. G. Scanlon, Jr., J. P. Fellner, R. A. Vaia, S. Vasudevan and E. P. Giannelis, "Polymer nanocomposites: a new strategy for synthesising solid electrolytes for rechargeable lithium batteries", *J. Power Sources*, 1995, **54**, 310–315.
- [25] F. Croce, G. B. Appetecchi, L. Persi and B. Scrosati, "Nanocomposite polymer electrolytes for lithium batteries", *Nature*, 1998, **394**, 456–458.
- [26] C. Capiglia, P. Mustarelli, E. Quartarone, C. Tomasi and A. Magistris, "Effects of nanoscale SiO<sub>2</sub> on the thermal and transport properties of solvent-free, poly(ethylene oxide) (PEO)-based polymer electrolytes", *Solid State Ionics*, 1999, **118**, 73–79.
- [27] J. Płocharski and W. Wiczorek, "PEO based composite solid electrolyte containing NASICON", *Solid State Ionics*, 1988, **28–30**, 979–982.
- [28] M. S. Michael, M. M. E. Jacob, S. R. S. Prabaharan and S. Radhakrishna, "Enhanced lithium ion transport in PEO-based solid polymer electrolytes employing a novel class of plasticizers", *Solid State Ionics*, 1997, **98**, 167–174.
- [29] H. Y. Sun, Y. Takeda, N. Imanishi, O. Yamamoto and H.-J. Sohn, "Ferroelectric materials as a ceramic filler in solid composite polyethylene oxide-based electrolytes", *J. Electrochem. Soc.*, 2000, **147**, 2462–2467.
- [30] W. Wiczorek, P. Lipka, G. Žukovska and H. Wyciślik, "Ionic interactions in polymeric electrolytes based on low molecular weight poly(ethylene glycol)s", *J. Phys. Chem. B*, 1998, **102**, 6968–6974.
- [31] W. Wiczorek, K. Such, H. Wyciślik and J. Płocharski, "Modifications of crystalline structure of PEO polymer electrolytes with ceramic additives", *Solid State Ionics*, 1989, **36**, 255–257.
- [32] A. S. Best, A. Ferry, D. R. MacFarlane and M. Forsyth, "Conductivity in amorphous polyether nanocomposite materials", *Solid State Ionics*, 1999, **126**, 269–276.
- [33] J. Przyłuski, M. Siekiński and W. Wiczorek, "Effective medium theory in studies of conductivity of composite polymeric electrolytes", *Electrochimica Acta*, 1995, **40**, 2101–2108.



- [34] H. Y. Sun, H.-J. Sohn, O. Yamamoto, Y. Takeda and N. Imanishi, "Enhanced lithium-ion transport in PEO-based composite polymer electrolytes with ferroelectric BaTiO<sub>3</sub>", *J. Electrochem. Soc.*, 1999, **146**, 1672–1676.
- [35] L. Edman, A. Ferry and P. Jacobsson, "Effect of C<sub>60</sub> as a filler on the morphology of polymer-salt complexes based on poly(ethylene oxide) and LiCF<sub>3</sub>SO<sub>3</sub>", *Macromolecules*, 1999, **32**, 4130–4133.
- [36] E. Strauss, D. Golodnitsky, G. Ardel and E. Peled, "Charge and mass transport properties of LiI-P(EO)<sub>n</sub>-Al<sub>2</sub>O<sub>3</sub>-based composite polymer electrolytes", *Electrochimica Acta*, 1998, **43**, 1315–1320.
- [37] "CACHe Computer Aided Chemistry. An online molecular modelling tutorial", University of Oxford, <http://www.chem.ox.ac.uk/course/cache/default.html>.
- [38] F. Ercolessi, "A molecular dynamics primer", Spring College in Computational Physics, ICTP, Trieste, June 1997, <http://www.fisica.uniud.it/~ercolessi/md/md/>.
- [39] D. C. Rapaport, "The Art of Molecular Dynamics Simulation", Cambridge University Press, 1995.
- [40] M. P. Allen and D. J. Tildesley, "Computer Simulation of Liquids", Oxford University Press, 1989.
- [41] D. W. Brenner, "Analytic potentials and molecular dynamics simulation", a part of the tutorial on "Critical Enabling Technologies for Nanotechnology", *Fifth Foresight Conference on Molecular Nanotechnology*, November 5, 1997, <http://www.mse.ncsu.edu/CompMatSci/Tutorial/>.
- [42] T. C. Huang, W. Parris, N. Masciocchi and P. W. Wang, "Derivation of d-values from digitized X-ray and synchrotron data", *Adv. X-Ray Anal.*, 1990, **33**, 295–303.
- [43] International Tables for Crystallography. Vol. A, ed. T. Hahn, *4th revised edition*, 1996.
- [44] J.-S. Soetens, C. Millot and B. Maigret, "Molecular dynamics simulation of Li<sup>+</sup>BF<sub>4</sub><sup>-</sup> in ethylene carbonate, propylene carbonate and dimethyl carbonate solvents", *J. Phys. Chem. A*, 1998, **102**, 1055–1061.
- [45] A. R. Leach, "Molecular Modelling. Principles and Applications", Longman, 1996.

- [46] The DL\_POLY Project, W. Smith and T. Forester, TCS Division, Daresbury Laboratory, Daresbury, Warrington WA44AD, England.
- [47] S. Neyertz, D. Brown and J. O. Thomas, "Molecular dynamics simulation of crystalline poly(ethylene oxide)", *J. Chem. Phys.*, 1994, **101**, 10064–10073.
- [48] S. Edvardsson, M. Klintonberg and J. O. Thomas, "Use of polarized optical absorption to obtain structural information for  $\text{Na}^+/\text{Nd}^{3+}$   $\beta''$ -alumina", *Phys. Rev. B*, 1996, **54**, 17476–17485.
- [49] P. Johansson. *Private communication*.
- [50] A. K. Rappe, C. J. Casewit, K. S. Colwell, W. A. Goddard III and W. M. Skiff, "UFF, a full periodic table force field for molecular mechanics and molecular dynamics simulations", *J. Amer. Chem. Soc.*, 1992, **114**, 10024–10035.
- [51] G. D. Smith, R. L. Jaffe and H. Partridge, "Quantum chemistry study of the Interactions of  $\text{Li}^+$ ,  $\text{Cl}^-$ , and  $\text{I}^-$  ions with model ethers", *J. Phys. Chem. A*, 1997, **101**, 1705–1715.
- [52] W. Wiczorek and M. Siekierski, "A description of the temperature dependence of the conductivity for composite polymeric electrolytes by effective medium theory", *J. Appl. Phys.*, 1994, **76**, 2220–2226.
- [53] W. Wiczorek, Z. Florjanczyk and J. R. Stevens, "Composite polyether based solid electrolytes", *Electrochimica Acta*, 1995, **40**, 2251–2258.
- [54] B. Scrosati, F. Croce and L. Persi, "Impedance spectroscopy study of PEO-based nanocomposite electrolytes", *J. Electrochem. Soc.*, 2000, **147**, 1718–1721.
- [55] F. Croce, L. Persi, F. Ronci and B. Scrosati, "Nanocomposite polymer electrolytes and their impact on the lithium battery technology", *Solid State Ionics*, 2000, **135**, 47–52.
- [56] A. Magistris, P. Mustarelli, E. Quartarone and C. Tomasi, "Transport and thermal properties of  $(\text{PEO})_n$ - $\text{LiPF}_6$  electrolytes for super-ambient applications", *Solid State Ionics*, 2000, **136–137**, 1241–1247.
- [57] E. A. Rietman, M. L. Kaplan and R. J. Cava, "Lithium ion-poly(ethylene oxide) complexes. I. Effect of anion on conductivity", *Solid State Ionics*, 1985, **17**, 67–73.

- [58] F. Müller-Plathe, “Permeation of polymers — a computational approach”, *Acta Polymerica*, 1994, **45**, 259–293.
- [59] M. Kakihana, S. Schantz and L. M. Torell, “Dissociated ions and ion-ion interactions in poly(ethylene oxide) based  $\text{NaCF}_3\text{SO}_3$  complexes”, *Solid State Ionics*, 1990, **40–41**, 641–644.
- [60] M. Forsyth, V. A. Payne, M. A. Ratner, S. W. de Leeuw and D. F. Shriver, “Molecular dynamics simulations of highly concentrated salt solutions: structural and transport effects in polymer electrolytes”, *Solid State Ionics*, 1992, **53–56**, 1011–1026.
- [61] L. Xie and G. C. Farrington, “Molecular mechanics and dynamics simulation of poly(ethylene oxide) electrolytes”, *Solid State Ionics*, 1992, **53–56**, 1054–1058.
- [62] F. Müller-Plathe and W. F. van Gunsteren, “Computer simulation of a polymer electrolyte: Lithium iodide in amorphous poly(ethylene oxide)”, *J. Physical Chemistry*, 1995, **103**, 4745–4756.
- [63] S. Neyertz and J. O. Thomas, “Molecular dynamics simulations of the amorphous polymer electrolyte  $\text{PEO}_x\text{NaI}$ ”, *Computational Polymer Science*, 1995, **5**, 107–120.
- [64] A. S. Best, “Lithium-ion conducting electrolytes for use in Lithium Battery Applications”, Thesis for the degree of *Doctor of Philosophy*, Monash University, Australia, 2001.
- [65] P. Johansson and P. Jacobsson, “ $\text{TiO}_2$  nano-particles in polymer electrolytes: surface interactions”, *In press*.
- [66] G. S. MacGlashan, Y. G. Andreev and P. G. Bruce, “Structure of the polymer electrolyte poly(ethylene oxide) $_6$ : $\text{LiAsF}_6$ ”, *Nature*, 1999, **398**, 792–794.
- [67] Z. Gadjourova, Y. G. Andreev, D. P. Tunstall and P. G. Bruce, “Ionic conductivity in crystalline polymer electrolytes”, *Nature*, 2001, **412**, 520–523.
- [68] Z. Gadjourova, D. M. y Marero, K. H. Andersen, Y. G. Andreev and P. G. Bruce, “Structures of the polymer electrolyte complexes  $\text{PEO}_6$ : $\text{LiXF}_6$  (X = P, Sb), determined from neutron powder diffraction data”, *Chem. Mater.*, 2001, **13**, 1282–1285.
- [69] Z. Stoeva, I. Martin-Litas, E. Staunton, Y. G. Andreev and P. G. Bruce, “Ionic conductivity in the crystalline polymer electrolytes  $\text{PEO}_6$ : $\text{LiXF}_6$ , X=P, As, Sb”, *In press*.

## **PUBLICATIONS**

*Heiki Kasemagi Ph. D. Thesis*

**I**

*Heiki Kasemagi Ph. D. Thesis*

# Molecular dynamics simulation of the effect of adding an Al<sub>2</sub>O<sub>3</sub> nanoparticle to PEO–LiCl/LiBr/LiI systems

Heiki Kasemägi,<sup>a,d</sup> Mattias Klintenberg,<sup>b,c</sup> Alvo Aabloo<sup>a</sup> and John O. Thomas<sup>\*d</sup>

<sup>a</sup>Technology Centre, Tartu University, Tähe 4, 51010 Tartu, Estonia

<sup>b</sup>Condensed Matter Theory Group, Department of Physics, Uppsala University, Box 530, SE-751 21 Uppsala, Sweden

<sup>c</sup>Lawrence Berkeley National Laboratory, University of California, Berkeley, USA

<sup>d</sup>Materials Chemistry, Ångström Laboratory, Uppsala University, Box 538, SE-751 21 Uppsala, Sweden. E-mail: josh.thomas@mkem.uu.se

Received 14th August 2001, Accepted 4th September 2001

First published as an Advance Article on the web 7th November 2001

The effect of adding *ca.* 20 Å diameter quasi-spherical nanoparticles of  $\alpha$ -Al<sub>2</sub>O<sub>3</sub> (corundum) to LiCl, LiBr and LiI salts in amorphous PEO has been simulated at a nominal 360 K by molecular dynamics (MD) methods; the Li:EO ratio studied was 1:10, along with salt-free and particle-free reference cases. The PEO forms an immobilised coordination sphere around the particle. Li-ion mobility in PEO is found to decrease on the addition of particles; the effect is greatest near the particle surface in the region of the PEO. LiX pairing/clustering (for X = Cl, Br, I) was observed away from the particle surface; the effect was greatest for LiBr and least for LiCl. The ion-clustering tendency would appear to be dependent on the particle size; it is noticeably larger for the case of smaller particles. A number of unpaired Li ions were found attached to the particle within the region of the immobilised PEO. Corresponding “free” anions were located somewhat further away from the particle surface in the more mobile PEO regions, along with charged and uncharged ion-clusters.

## Introduction

Poly(ethylene oxide) (PEO)-based polymer electrolytes have been the object of considerable interest for several decades, mainly through their potential use as polymer electrolytes in electrochemical devices. However, at ambient temperatures, PEO-based electrolytes are generally poor ion conductors ( $\sigma < 10^{-8} \text{ S cm}^{-1}$ ) due to their high degree of local crystallinity.<sup>1</sup> A number of salts, *e.g.* RbSCN, RbI, CsSCN, CsI and Hg(ClO<sub>4</sub>)<sub>2</sub>, actually form low-temperature amorphous phases with PEO at relatively high salt concentrations but, with the major interest centred on lithium-based electrochemical devices, amorphous lithium-salt/polymer electrolytes are desirable. Reasonable conductivity in lithium-salt/PEO electrolytes can be achieved (*ca.*  $10^{-5} \text{ S cm}^{-1}$ ) around 100 °C, but the mechanical properties of these polymer materials are poor.

There has therefore been a strong focus in recent years on obtaining improved ambient temperature Li-ion conductivity, improved mechanical stability, and electrochemical stability with respect to active electrode materials. Most recently, attention has turned to the incorporation of nanosize particles into ionically conducting polymers in order to improve their ion conductivities. For example, Krawiec *et al.*<sup>2</sup> found that adding nanosize particles of  $\alpha$ -Al<sub>2</sub>O<sub>3</sub> to (PEO)<sub>8</sub> LiBF<sub>4</sub> increased its conductivity by an order of magnitude compared to that obtained using micron-size particles. This conductivity enhancement has been found to be dependent on filler concentration; maximum ionic conductivity was obtained for 10 wt.% nanosize Al<sub>2</sub>O<sub>3</sub>. Croce *et al.*<sup>3</sup> could demonstrate conductivity enhancement in PEO–LiClO<sub>4</sub> mixtures containing both TiO<sub>2</sub> and Al<sub>2</sub>O<sub>3</sub> nanoparticles (diameter 6–130 Å) in the temperature range of 30–80 °C. It was later shown by Capiglia *et al.*<sup>4</sup> that the addition of nanoscale SiO<sub>2</sub> filler-particles to the (PEO)<sub>8</sub>–LiClO<sub>4</sub> and (PEO)<sub>8</sub>–LiN(CF<sub>3</sub>SO<sub>2</sub>)<sub>2</sub> systems increases the conductivity by more than an order of magnitude; the effect was again shown to be filler-concentration dependent. It was

also claimed by Sun *et al.*<sup>5</sup> that the addition of micron-size particles of the ferroelectric BaTiO<sub>3</sub> (diameter: 0.6–1.2 µm) to PEO–LiClO<sub>4</sub> enhanced its ionic conductivity.

The effect of salt concentration under constant filler-concentration condition has been studied by Best *et al.*<sup>6</sup> An amorphous polyether triol with ethylene and propylene oxide units in 3:1 ratio (3PEG) was studied for LiClO<sub>4</sub> and LiN(CF<sub>3</sub>SO<sub>2</sub>)<sub>2</sub> (LiTFSI) in different concentrations, and 10 wt.% TiO<sub>2</sub> filler. The filler appears to increase the conductivity at higher salt concentrations. This was suggested to occur for the case of LiClO<sub>4</sub> by lowering the degree of ion aggregation within the polymer–salt mixture as a result of competing interactions between salt-ions and filler. This was explained in the case of LiTFSI by a lower degree of ion aggregation. On the other hand, Wiczorek *et al.*<sup>7</sup> have shown that the conductivity increases with salt concentration in the low molecular weight poly(ethylene glycol) (PEG)–LiClO<sub>4</sub> system with  $\alpha$ -Al<sub>2</sub>O<sub>3</sub> nanoparticles as filler. The conductivity was shown by Strauss *et al.*<sup>8</sup> to reach a maximum at *n* = 20 in the LiI–(PEO)<sub>*n*</sub>–Al<sub>2</sub>O<sub>3</sub> system. Also, more ion-pairs were found in the composite polymer electrolyte case; these pairs reduce the effective concentration of charge carriers and contribute an additional term in the diffusion impedance.

A number of molecular dynamics (MD) simulations have been made by our group of the properties of crystalline<sup>9</sup> and amorphous<sup>10</sup> PEO containing various lithium-salt ions; and of surface properties of related PEO–salt systems.<sup>11–13</sup> The aim of this paper is to provide some deeper insights into the behaviour of nano-composite polymer electrolytes. This we achieve by simulating a series of models involving amorphous PEO containing Li salts and nanosize Al<sub>2</sub>O<sub>3</sub> (corundum) particles. Models involving amorphous PEO alone, and PEO with salt or filler alone are studied as reference states. MD simulations were made for LiCl, LiBr and LiI as dopant salts for an Li:EO ratio of 1:10.

## The models

Neutral pieces of  $\alpha$ -Al<sub>2</sub>O<sub>3</sub> (corundum) were extracted from its rhombohedral crystal structure (space group:  $R\bar{3}c$  (no. 167);<sup>14</sup> unit-cell parameters:  $a=4.75$  Å,  $c=12.99$  Å (hexagonal setting)).<sup>15</sup> These particles were then “computer-annealed” at 2000 K to give them roughly spherical forms (diameters: 14 Å and 18 Å; 115 and 335 atoms, respectively) and with oxygen atoms at their surfaces. The simulation boxes were then filled with PEO by controlled pivotal Monte Carlo growth around the particles.

A total of 12 models were simulated: two particle-sizes (14 Å and 18 Å); three salts (LiCl, LiBr and LiI); and six reference states (PEO alone, PEO with two particle-sizes and no salt, PEO with three salts and no particle). The simulation boxes were as follows:

(1) A rectangular particle-free and salt-free reference box ( $26 \times 21 \times 22$  Å) containing an amorphous PEO chain of 200 EO monomers.

(2) Cubic reference simulation boxes containing particles:

(1) box size  $31 \times 31 \times 31$  Å;  $\sim 14$  Å diameter particle; 455 EO monomers;

(2) box size  $37 \times 37 \times 37$  Å;  $\sim 18$  Å diameter particle; 787 EO monomers.

(3) A rectangular particle-free reference box ( $26 \times 21 \times 22$  Å) containing an amorphous PEO chain of 200 EO monomers and three different lithium-salts.

(4) Cubic simulation boxes containing PEO, salt and particle:

(1) box size  $31 \times 31 \times 31$  Å; 14 Å diameter particle; 455 EO monomers; *ca.* 6% of the total volume, and 10% of the total mass were occupied by the particle; the particle surface-area was  $300 \text{ m}^2 \text{ cm}^{-3}$ .

(2) box size  $37 \times 37 \times 37$  Å; 18 Å diameter particle; 787 EO monomers; particle filling was here *ca.* 10% of the total volume and 16% of the total mass; the particle surface-area was  $600 \text{ m}^2 \text{ cm}^{-3}$ .

The simulation box sizes were chosen to leave the minimum distance between the particle surfaces in the periodic arrangement of particles the same as the particle diameters in the two cases. Unpaired lithium-salt ions were inserted randomly into the PEO host with an Li:EO ratio of 1:10.

## The molecular dynamics (MD) simulation method

MD simulation involves the simultaneous solution of Newton's equations of motion for all atoms (or ions) in an appropriately chosen simulation box. A local version of DL-POLY<sup>16</sup> with force fields developed earlier for PEO,<sup>9</sup>  $\beta$ -alumina,<sup>17</sup> LiBr and Br-PEO,<sup>18,19</sup> LiCl, LiI, Li-PEO, Cl-PEO and I-PEO.<sup>20</sup> The long-range interaction potentials were described by eqn. (1):

$$U(r) = A \exp\left(-\frac{B}{r}\right) - \frac{C}{r^6} - \frac{D}{r^4} + \frac{q_1 q_2}{4\pi\epsilon_0 r} \quad (1)$$

The parameters used are listed in Table 1.

The MD simulations used periodic boundary conditions and an Ewald summation to calculate the electrostatic forces at longer distances. Each simulation consisted of an equilibration period of 50 ps followed by  $NVT$  simulation (number of particles ( $N$ ), volume ( $V$ ) and temperature ( $T$ ) constant) for 100 ps, followed by  $NpT$  simulation (Nosé-Hoover model:  $N$ , pressure ( $p$ ) and  $T$  constant) for up to 800 ps at nominal temperature 360 K. Sampling was made every 1 ps (every 1000 time-steps) in the simulation. Models were prepared on a local array of PCs, and the MD simulations carried out on an IBM Power Parallel SP supercomputer at the Parallel Computer Centre (PDC) of the Royal Institute of Technology (KTH) in Stockholm; a total of 36000 CPU hours was used.

**Table 1** Potential parameters describing the long-range interactions ( $O_{\text{et}}$ : ether oxygen;  $O_{\text{Al}}$ : particle oxygen)

Atom pair	$A/$ kcal mol <sup>-1</sup>	$B/\text{Å}$	$C/$ kcal Å <sup>6</sup> mol <sup>-1</sup>	$D/$ kcal Å <sup>4</sup> mol <sup>-1</sup>
$O_{\text{et}} \cdots O_{\text{et}}$	58298.9	0.24849	192.1	0.0
$O_{\text{et}} \cdots C$	42931.6	0.27550	352.8	0.0
$O_{\text{et}} \cdots H$	20432.6	0.24450	98.8	0.0
$O_{\text{et}} \cdots \text{Al}$	928077.6	0.24997	1139.9	0.0
$O_{\text{et}} \cdots O_{\text{Al}}$	951969.6	0.15784	239.7	0.0
$C \cdots C$	31615.1	0.30251	647.8	0.0
$C \cdots H$	15046.7	0.27151	181.5	0.0
$C \cdots \text{Al}$	170201.1	0.30315	2160.9	0.0
$C \cdots O_{\text{Al}}$	1172167.0	0.24855	4537.0	0.0
$H \cdots H$	7161.2	0.24050	50.8	0.0
$H \cdots \text{Al}$	110177.8	0.26812	669.5	0.0
$H \cdots O_{\text{Al}}$	998796.7	0.19945	919.0	0.0
$\text{Al} \cdots \text{Al}$	0.0	0.10000	0.0	0.0
$\text{Al} \cdots O_{\text{Al}}$	33652.8	0.29912	0.0	0.0
$O_{\text{Al}} \cdots O_{\text{Al}}$	524957.1	0.14900	530.4	0.0
$\text{Li} \cdots O_{\text{et}}$	191106.0	0.17510	0.0	76.9
$\text{Li} \cdots C$	8140.0	0.37994	0.0	76.9
$\text{Li} \cdots H$	13139.0	0.22852	0.0	77.4
$\text{Li} \cdots \text{Al}$	5308294.0	0.14873	0.0	0.0
$\text{Li} \cdots O_{\text{Al}}$	62774060.0	0.11668	0.0	0.0
$\text{Li} \cdots \text{Li}$	44195.0	0.13742	0.0	9.3
$\text{Li} \cdots \text{Br}$	30563.7	0.39879	0.0	2916.7
$\text{Li} \cdots \text{Cl}$	30868.0	0.31797	0.0	729.4
$\text{Li} \cdots \text{I}$	23625.0	0.41034	0.0	2108.7
$\text{Br} \cdots O_{\text{et}}$	50059.4	0.30488	313.1	621.4
$\text{Br} \cdots C$	18714.6	0.39014	3099.2	20.7
$\text{Br} \cdots H$	8234.8	0.34214	391.8	0.0
$\text{Br} \cdots O_{\text{Al}}$	40369390.0	0.15673	2263.9	0.0
$\text{Br} \cdots \text{Al}$	2958746.0	0.27148	13428.4	0.0
$\text{Br} \cdots \text{Br}$	195631400.0	0.19305	0.0	2149.8
$\text{Cl} \cdots O_{\text{et}}$	40353.0	0.31056	1005.0	536.3
$\text{Cl} \cdots C$	17926.0	0.36590	1273.3	67.2
$\text{Cl} \cdots H$	7543.0	0.32701	263.0	0.0
$\text{Cl} \cdots O_{\text{Al}}$	654978.0	0.23133	491.7	0.0
$\text{Cl} \cdots \text{Al}$	2633313.0	0.27671	14322.4	0.0
$\text{Cl} \cdots \text{Cl}$	70768.4	0.39622	29699.1	0.0
$\text{I} \cdots O_{\text{et}}$	52238.0	0.33910	2604.0	712.4
$\text{I} \cdots C$	23213.0	0.40617	3301.0	77.7
$\text{I} \cdots H$	9764.0	0.35881	682.5	0.0
$\text{I} \cdots O_{\text{Al}}$	40369390.0	0.14686	3619.7	0.0
$\text{I} \cdots \text{Al}$	3236445.0	0.28076	19481.8	0.0
$\text{I} \cdots \text{I}$	1898731000.0	0.17742	0.0	2734.4

## Results and discussion

### Structural effects

The ultimate purpose of this work is to study the influence of nanosize inorganic particles on the salt-in-PEO system (Fig. 1). Let us first consider, however, the changes in the particle and PEO structure after adding the nanoparticle and the salt to PEO (particles of 14 Å diameter and 18 Å diameter will be referred to hereafter as 14 Å and 18 Å particles).

We see from Fig. 2 that the surface of the generated 18 Å particle is well defined, with  $O_{\text{Al}}$  atoms tending to lie outermost with five-fold  $\text{Al}-O_{\text{Al}}$  coordination. In corundum, the  $\text{Al}-O_{\text{Al}}$  coordination is six-fold, but we see that the radial distribution function for the particle (Fig. 3) shows average coordination number to be five. This is because the simulated particle is of nanosize and is thus essentially “all-surface and no-bulk”. This distribution is found to remain virtually unchanged for both the particle-in-PEO and particle-in-salt-in-PEO systems.

Let us consider now what happens to the PEO host structure on adding the nanosize particle. There is clearly a region of high ether-oxygen ( $O_{\text{et}}$ ) concentration *ca.* 3 Å outside the particle surface for both particle radii (Fig. 4). The polymer chain tends to curl itself around the particle to form a “coordination sphere” (Fig. 5(a)). Note that this effect is not a result of the polymer simply being forced away from the inserted particle; on the contrary, the polymer was generated so



Fig. 1 Simulation box for the case of a 14 Å diameter  $\text{Al}_2\text{O}_3$  particle in amorphous  $\text{LiCl}(\text{PEO})_{10}$ .

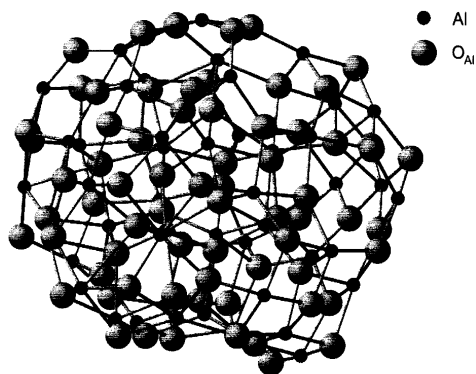


Fig. 2 Atomic-level structure of the 14 Å diameter  $\text{Al}_2\text{O}_3$  particle after simulated annealing.

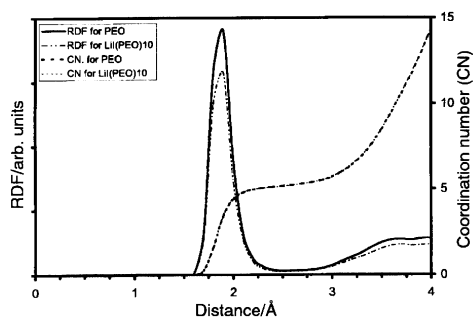


Fig. 3 Radial distribution function for  $\text{Al}\cdots\text{O}_{\text{Al}}$  for the case of the 18 Å particle in PEO and  $\text{LiI}(\text{PEO})_{10}$  ( $\text{O}_{\text{Al}}$  - particle oxygen).

as to fill the space left in the simulation box around the particle. Note also that it is not a continuous section on PEO that curls itself around the particle, but rather that the same chain approaches and leaves the particle at several points along its length, with up to five successive  $\text{O}_{\text{e}}$  atoms in close proximity to the particle.

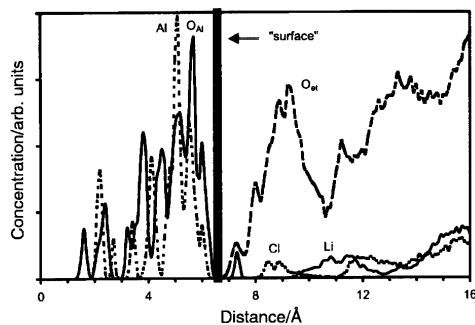


Fig. 4 Atom density distribution for the 14 Å diameter  $\text{Al}_2\text{O}_3$  particle in  $\text{LiCl}(\text{PEO})_{10}$ .

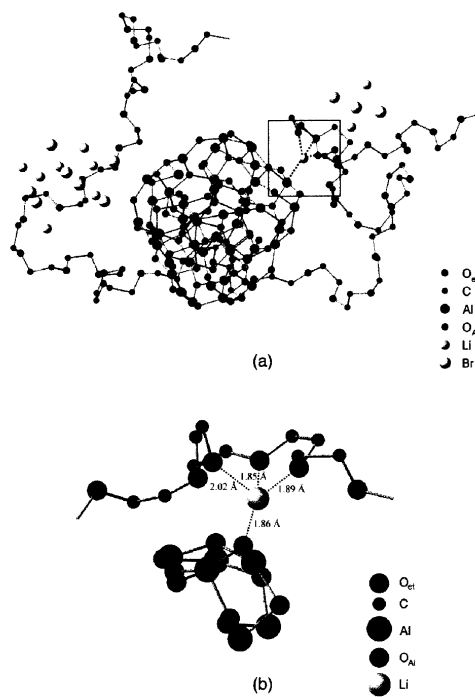


Fig. 5 (a) PEO chain around the 14 Å particle with Li- and Br-ions; (b) an example of the detailed structure around a  $\text{Li}^+$  ion bound to the particle.

So now to the effect of adding salt to PEO: we have studied three monoatomic anion cases:  $\text{LiX}(\text{PEO})_{10}$  for  $\text{X}=\text{Cl}$ ,  $\text{Br}$  and  $\text{I}$ ; in practice, more complex polyatomic anions like  $\text{BF}_4^-$ ,  $\text{PF}_6^-$ , "triflate"  $[\text{CF}_3\text{SO}_3^-]$  and "TFSI"  $[\text{N}(\text{CF}_3\text{SO}_2)_2^-]$  are more commonly exploited in a battery context, due largely to their less concentrated distribution of negative charge. Li-X radial distribution functions (RDFs) are seen to have sharp first peaks at 2.25, 2.50 and 2.70 Å for LiCl, LiBr and LiI, respectively (see Fig. 6 for LiI results). The coordination numbers (CN) show clear plateaus corresponding to these peaks at 1.5 for LiCl, 2.4 for LiI (Fig. 6), and 2.7 for LiBr. This suggests a tendency to form ion-clusters for LiI and LiBr and ion-pairs and -clusters for LiCl. Similar clustering tendencies have been seen in simulations of LiI in  $(\text{PEO})_x\text{LiI}$  ( $x=100, 50, 25, 16$  and



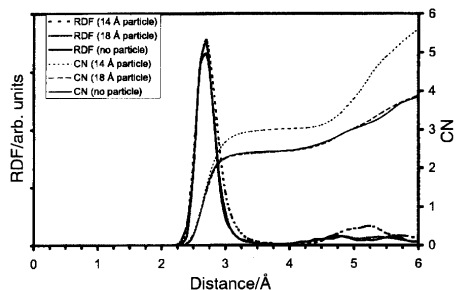


Fig. 6 Radial distribution function for Li...I for the case of LiI(PEO)<sub>10</sub> and 14 Å and 18 Å particles in LiI(PEO)<sub>10</sub>.

8) by Müller-Plathe and van Gunsteren,<sup>21</sup> ion-pairing has also been observed for LiClO<sub>4</sub> in MD simulations of amorphous PEO by Halley *et al.*<sup>22</sup>

The most interesting phenomena to probe are, of course, those resulting from adding the particle to the salt-in-PEO system. Some dissociated lithium ions are found to collect between the particle surface and the surrounding PEO. An example of the local environment of one such lithium ion is shown in Fig. 5(b); it coordinates to three O<sub>ct</sub> atoms and to one particle-oxygen O<sub>Al</sub> which is, in turn, itself two-fold coordinated to Al-atoms.

The ion-pairing and -clustering effects discussed above for the salt-in-PEO system increase on adding the particle; the coordination number for LiI is higher after adding the 14 Å particle to the salt-in-PEO system (Fig. 6); rising from 2.45 to 3.0. While a few lithium ions are found near the particle surface, the remaining lithiums and most of the anions participate in cluster- and pair-formation away from the particle (Fig. 4). Only very few anions can be considered as “free” and not belonging to any ion-cluster or ion-pair. Cluster sizes vary greatly, involving from 3 to as many as 30 ions for the 14 Å particle case (Fig. 7). The clusters are either neutral or carry +1 to -2 charges. One of the main effects of adding the

particle is thus to increase ion-association. The clusters tend to contain more ions on the addition of a particle than in the salt-in-PEO cases alone, and these clusters are located away from the particle.

### Dynamical effects

The dynamical effects of adding a nanoparticle to the salt-in-PEO system can also be extracted from the MD simulations. We see, not surprisingly, that the Al and O<sub>Al</sub> atoms vibrate somewhat more at the particle surface than near its centre (Fig. 8), and that this effect is virtually unchanged between the particle-in-PEO and particle-in-salt-in-PEO cases. The effect of both polymer and salt on atomic-level motion in the particle is clearly negligible.

The same cannot be said of the effect of the particle on PEO dynamics; the PEO chain is clearly immobilised in its “coordination sphere” around the particle (Fig. 9), considerably more mobile away from the particle; but still less mobile than in particle-free PEO. Interestingly, the ether-oxygens are seen to be more mobile both near and “away from” the 18 Å particle than the 14 Å particle. This could well be an unfortunate

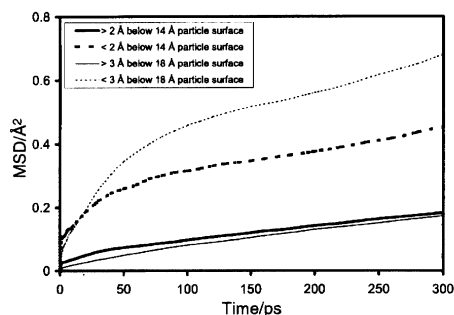


Fig. 8 Mean-square-displacement (MSD) for Al for the cases of 14 Å and 18 Å particles in PEO.

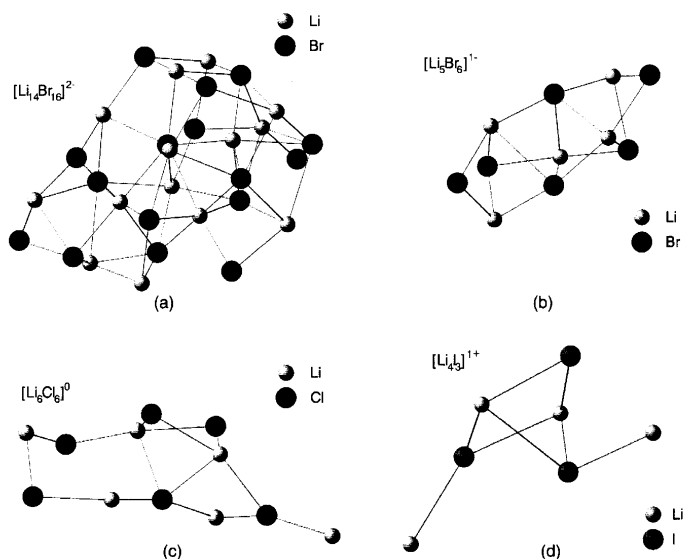


Fig. 7 Examples of ion-clustering: (a) [Li<sub>4</sub>Br<sub>16</sub>]<sup>2-</sup> for a 14 Å particle; (b) [Li<sub>5</sub>Br<sub>6</sub>]<sup>1-</sup> for a 14 Å particle; (c) [Li<sub>6</sub>Cl<sub>6</sub>]<sup>0</sup> for a 14 Å particle; (d) [Li<sub>4</sub>I<sub>3</sub>]<sup>1+</sup> for an 18 Å particle.

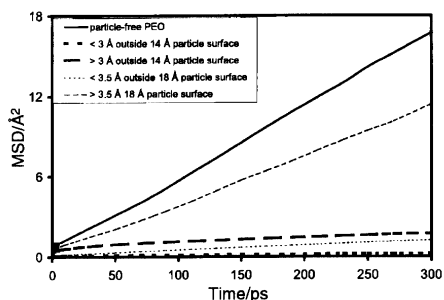


Fig. 9 Mean-square-displacements for ether O atoms in the case of 14 Å and 18 Å diameter  $\text{Al}_2\text{O}_3$  particles in PEO.

artefact of the arbitrary condition that the distance between the particles is equal to the particle diameter, since we must have more “bulk” PEO in the 18 Å particle case. The “coordination sphere” remains rigid and immobilised in all simulated systems. This “rigid coordination sphere” formed around the particle appears to expel most of the ions to regions away from the particle surface, thus causing the relative increase in ionic concentration away from the particle surface and consequent higher ion-clustering effects; a small number of lithium ions remain bonded to the particle.

We also see that lithium ions show higher mobility in the salt-in-PEO than in the particle-in-salt-in-PEO cases, with a minimal Li-ion mobility near the particle surface, and higher Li-ion mobility away from the particle surface; but still not approaching the Li-ion mobility in the particle-free cases (Fig. 10). Also, Li-ion mobility in the PEO tends to be higher away from the larger particle. Moreover, the mobilities for  $\text{Cl}^-$ ,  $\text{Br}^-$  and  $\text{I}^-$  anions tend to be comparable to and, in some cases, even higher than those of the lithium ions.

## Conclusions

The results presented here are an excellent illustration of what can realistically be achieved through MD simulation of a system of this relative complexity, although they perhaps do not give any absolutely definitive answers. A number of clear qualitative observations can be made:

(1) The most reliable indications to emerge are of the immobilisation of a small number of  $\text{Li}^+$  ions (ca. 3–5) near the surface of the nanoparticle. We also see that the clusters formed (although they can be large) will tend to be either neutral or carry a small excess charge (+2 to -1) (see the histogram in Fig. 11). The simulations made here give no indication as to the dissociation properties of these clusters as they approach the

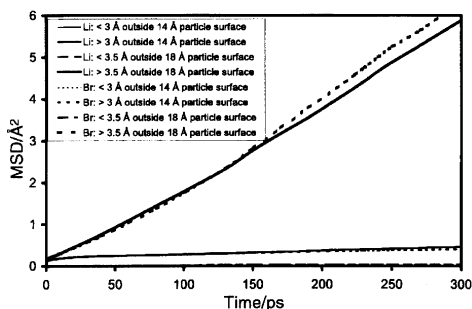


Fig. 10 Mean-square-displacement for  $\text{Li}^+$  and  $\text{Br}^-$  ions for the cases of 14 Å and 18 Å particles in  $\text{LiBr}(\text{PEO})_{10}$ .

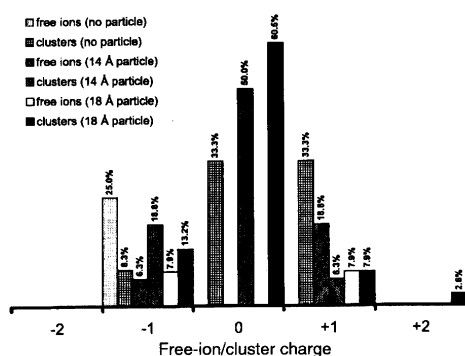


Fig. 11 A histogram showing the distribution of free-ion/cluster charges for the  $\text{LiCl}$  systems.

electrolyte–electrode interface. It is actually this which controls the battery-related properties of a given polymer–salt–electrode combination.

(2) This  $\text{Li}^+$  immobilisation has a significant secondary effect; namely, that these bound lithiums also attract and coordinate the  $\text{O}_{\text{et}}$  atoms of the PEO chain, resulting in regions of immobilised PEO in a “coordination shell” around the nanoparticle. Although successive  $\text{O}_{\text{et}}$  atoms along the PEO chain do not wrap themselves around the nanoparticle (the chain tends to make and break contact with the particle at several points along its length), the analogy with a “first hydration sphere” around a positive ion in a water–salt solution is clear. Outside this “first shell”, the PEO and salt ions are significantly more mobile.

(3) It is in these outer regions that the ion-pairing and ion-clustering phenomena appear, and it is apparent that these effects are significantly greater for the smaller diameter particle. More careful attention must be paid here to the choice of model parameters; it is also more relevant from a battery point of view to study polyatomic anions (triflate, imide,  $\text{PF}_6^-$ ,  $\text{BF}_4^-$ , etc.), in which the negative charges are more spatially dispersed over their surfaces, thereby rendering them less prone to ion-aggregation effects.

(4) One of the few pieces of solid experimental evidence of the effect of particle addition is the disappearance of the so-called DLAM-mode related to the damping of librational motion of the PEO, as the PEO becomes bound to the particle.<sup>6</sup> This is, indeed, well predicted by the simulation—where several sections along the PEO length (up to 5  $\text{O}_{\text{et}}$  atoms) are seen to become bound to the particle and essentially rigid. The naïve picture that this effect would expel excess positive charge into the PEO bulk would not appear to apply, however. It would rather appear that the immobilised PEO helps to bind positively charged Li ions near to the particle surface—thus expelling negative charge carriers into the PEO bulk. These simplistic pictures must be further probed in future studies, however.

In retrospect, we see then that there are many *model parameters* that could perhaps have been chosen in a more optimal manner to fully realise our original goal of actually probing the effect of adding a nanoparticle to a PEO–salt system, e.g.:

(1) the *salt concentration* could have been lower to avoid the serious ion-pairing and ion-clustering effects described above.

(2) the effective *simulation temperature* must also be carefully tuned: if set too high, we risk large ion-aggregation effects (as seen here); set too low, and the simulations take an unrealistically long calculation time. We see now that we may have chosen somewhat too high a simulation temperature (360 K); 300–320 K would perhaps have been optimal.

(3) parameters relating to *model geometry* (particularly particle and simulation-box dimensions) can also have had a decisive effect on the results which have emerged. We have here ensured that the minimum distance between the particles is the *same* as the chosen particle diameter. Other choices could have been made, and might well have led to qualitatively different results.

### Acknowledgements

This work has been supported by grants from the Swedish Natural Science Research Council (NFR), Stipendia to Heiki Kasemägi from the Nordic Energy Research Programme (NEFP), the Kami Research Foundation (KFS) and the Estonian Science Foundation (ETF) are all gratefully acknowledged, as is the fine service provided by the Stockholm Parallel Computer Centre (PDC). We also wish to thank Dr Patrik Johansson of CTH, Gothenburg for his force field parameters for LiBr.

### References

- 1 F. M. Gray, *Polymer Electrolytes*, The Royal Society of Chemistry, Cambridge, 1997.
- 2 W. Krawiec, L. G. Scanlon, Jr., J. P. Fellner, R. A. Vaia, S. Vasudevan and E. P. Giannelis, *J. Power Sources*, 1995, **54**, 310.
- 3 F. Croce, G. B. Appetecchi, L. Persi and B. Scrosati, *Nature*, 1998, **394**, 456.
- 4 C. Capiglia, P. Mustarelli, E. Quartarone, C. Tomasi and A. Magistris, *Solid State Ionics*, 1999, **118**, 73.
- 5 H. Y. Sun, H.-J. Sohn, O. Yamamoto, Y. Takeda and N. Imanishi, *J. Electrochem. Soc.*, 1999, **146**, 1672.
- 6 A. S. Best, A. Ferry, D. R. MacFarlane and M. Forsyth, *Solid State Ionics*, 1999, **126**, 269.
- 7 W. Wiczorek, P. Lipka, G. Zukowska and H. Wycilik, *J. Phys. Chem. B*, 1998, **102**, 6968.
- 8 E. Strauss, D. Golodnitsky, G. Ardel and E. Peled, *Electrochimica Acta*, 1998, **43**, 1315.
- 9 S. Neyertz, D. Brown and J. O. Thomas, *J. Chem. Phys.*, 1994, **101**, 10064.
- 10 S. Neyertz, D. Brown and J. O. Thomas, *Comput. Polym. Sci.*, 1995, **5**, 107.
- 11 A. Aabloo and J. O. Thomas, *Comput. Theor. Polym. Sci.*, 1997, **7**, 47.
- 12 A. Aabloo and J. O. Thomas, *Electrochim. Acta*, 1998, **43**, 1361.
- 13 A. Aabloo, M. Klintonberg and J. O. Thomas, *Electrochim. Acta*, 2000, **45**, 1425.
- 14 *International Tables for Crystallography, Vol. A: Space-Group Symmetry*, ed. T. Hahn, 4th revised edn., 1996.
- 15 T. C. Huang, W. Parrish, N. Masciocchi and P. W. Wang, *Adv. X-Ray Anal.*, 1990, **33**, 295.
- 16 The DL\_POLY Project, W. Smith and T. Forester, TCS Division, Daresbury Laboratory, Daresbury, Warrington WA4 4AD, England.
- 17 S. Edvardsson, M. Klintonberg and J. O. Thomas, *Phys. Rev. B*, 1996, **54**, 17476.
- 18 P. Johansson, personal communication.
- 19 A. K. Rappé, C. J. Casewit, K. S. Colwel, W. A. Goddard III and W. M. Skiff, *J. Am. Chem. Soc.*, 1992, **114**, 10024.
- 20 G. D. Smith, R. L. Jaffe and H. Partridge, *J. Phys. Chem. A*, 1997, **101**, 1705.
- 21 F. Müller-Plathe and W. F. van Gunsteren, *J. Chem. Phys.*, 1995, **103**, 4745.
- 22 J. W. Halley, Y. Duan, L. A. Curtiss and A. G. Baboul, *J. Chem. Phys.*, 1999, **111**, 3302.

# II

*Heiki Kasemagi Ph. D. Thesis*

## Molecular dynamics simulation of the $\text{LiBF}_4$ –PEO system containing $\text{Al}_2\text{O}_3$ nanoparticles

Heiki Kasemägi<sup>a,b</sup>, Mattias Klintonberg<sup>c,d</sup>, Alvo Aabloo<sup>a</sup>, John O. Thomas<sup>b,\*</sup>

<sup>a</sup>Technology Centre, Tartu University, Tähe 4, 51010 Tartu, Estonia

<sup>b</sup>Materials Chemistry, Ångström Laboratory, Uppsala University, Box 538, SE-751 21 Uppsala, Sweden

<sup>c</sup>Condensed Matter Theory Group, Department of Physics, Uppsala University, Box 534, SE-751 21 Uppsala, Sweden

<sup>d</sup>Lawrence Berkeley National Laboratory, University of California, Berkeley, CA 94720, USA

### Abstract

The amorphous  $\text{LiBF}_4(\text{PEO})_{20}$  system has been simulated alone and containing a ca. 14-Å diameter  $\text{Al}_2\text{O}_3$  nanoparticle and in juxtaposition with a ca. 65-Å thick  $\alpha$ - $\text{Al}_2\text{O}_3$  slab at a nominal temperature of 293 K by Molecular Dynamics (MD) methods. Li-ion mobility in the poly(ethylene oxide) (PEO) host is found to increase on the addition of the nanoparticle; the effect is also noticeable for the alumina slab. This can be seen as theoretical confirmation of the positive influence of nanoparticles on ion mobility in a PEO–salt system, as observed earlier experimentally. Other effects observed are related to this Li-ion mobility enhancement: PEO forms an immobilised coordination sphere around the particle and an immobilised layer at the surface of the  $\alpha$ -alumina slab. No Li ions are found near the particle or at the slab surface. Instead, two to three unpaired  $\text{BF}_4^-$  anions are found attached to the particle within the region of immobilised PEO and at least one is found immobilised on the slab surface, leaving free Li ions in the regions away from the particle and slab surfaces. No more than 60% of the Li ions form ion pairs and ion clusters in the regions away from the particle surface and up to 87% of the Li ions form ion pairs and ion clusters in the regions away from the slab surface. © 2002 Published by Elsevier Science B.V.

PACS: 82.20.Wt; 82.35.Np; 82.35.Rs

Keywords: Polymer battery; Polymer electrolytes; Nanofillers; Poly(ethylene oxide); Lithium tetrafluoroborate

### 1. Introduction

The secondary lithium-polymer battery is an important power source in a number of applications, e.g. in the communications and in the fast-growing electric vehicle sectors. Experimental and theoretical efforts have been focused to improve the performance of all parts of the battery. One of the clearest research

goals is to improve the conductivity and mechanical properties of the polymer electrolyte at ambient and elevated temperatures. We have here chosen poly(ethylene oxide) (PEO) as a host polymer in our model system because of its wide use as prototype polymer electrolyte; its properties and structure are, thus, well documented.

It is known that the Li-ion conductivity of PEO is generally quite poor at ambient temperatures due to the high degree of crystallinity [1]. Different methods have been used to improve its conductivity: adding organic [2,3] or inorganic plasticizers [4] to form a

\* Corresponding author. Fax: +46-18-513548.

E-mail address: josh.thomas@mkem.uu.se (J.O. Thomas).

PEO-based gel electrolyte, using lithium salts with different anion types [1]. Our research has focused on another strategy: the effect of adding nanosize inorganic particles (“nanoparticles”) to the PEO–lithium-salt system and especially its influence on ion conductivity at room temperature.

Experimental data show that inorganic nanoparticles increase ionic conductivity by up to an order of magnitude: adding TiO<sub>2</sub> and Al<sub>2</sub>O<sub>3</sub> nanoparticles to the LiClO<sub>4</sub>–PEO system increases ionic conductivity to 10<sup>−4</sup> S cm<sup>−1</sup> at 50 °C and 10<sup>−5</sup> S cm<sup>−1</sup> at 30 °C [5]. The effect of nanoparticles on ion conductivity has also been seen in the LiClO<sub>4</sub>–3PEG–TiO<sub>2</sub> system [6] and α-Al<sub>2</sub>O<sub>3</sub> nanoparticles increase conductivity in the LiBF<sub>4</sub>(PEO)<sub>8</sub> system at room temperature [7]. The effect of nanoparticles seems to depend on particle size and concentration. Nanoparticle diameters are usually in the range of 6–15 nm, but up to micron-size particles are also used [7]. Best results are seen at 10 wt.% filler [5,7,8].

Significant ion-clustering effects are seen in MD simulations of polymer systems containing lithium salts involving monoatomic anions [9]. On the other hand, lithium salts with polyatomic anions tend to exhibit little or no ion clustering. We also know from our previous simulations that ion clustering is temperature-dependent, increasing when the simulation temperature is above room temperature.

In this present work, we have simulated the PEO–LiBF<sub>4</sub> systems at room temperature with and without Al<sub>2</sub>O<sub>3</sub> nanoparticles and in juxtaposition with an α-Al<sub>2</sub>O<sub>3</sub> slab. The anion type and simulation temperature (293 K) has been chosen to avoid ion-clustering effects. The nanoparticle concentration was roughly chosen to reproduce experimental conditions, which have resulted in the highest ion conductivities. The PEO–LiBF<sub>4</sub>–Al<sub>2</sub>O<sub>3</sub> slab system was used to simulate the effect of adding a large α-Al<sub>2</sub>O<sub>3</sub> particle to the PEO–salt system.

## 2. The model

The simulation boxes were filled with PEO by controlled pivotal Monte Carlo growth. Lithium-salt ions and a nanoparticle were added into the simulation box prior to chain generation. Lithium tetrafluoroborate (LiBF<sub>4</sub>) was used as lithium salt; BF<sub>4</sub><sup>−</sup> was treated

as a rigid ion with B–F distance 1.39 Å and F–F distance 2.27 Å [10]. Salt ions were inserted randomly into the simulation box with an Li/EO ratio of 1:20. A neutral piece of α-Al<sub>2</sub>O<sub>3</sub> (corundum) was extracted from its rhombohedral crystal structure (space-group: R $\bar{3}c$  (No. 167) [11]; unit-cell parameters:  $a=4.75$  Å,  $c=12.99$  Å (hexagonal setting) [12]). The particle was then “computer annealed” at 2000 K to give it a roughly spherical form (diameter 14 Å; 115 atoms) with oxygen atoms predominantly at its surface.

Table 1  
Potential parameters describing the long-range interactions (O<sub>et</sub>: ether oxygen; O<sub>Al</sub>: particle oxygen)

Atom pair	A/kcal/mol	B/Å	C/kcal Å <sup>6</sup> /mol	D/kcal Å <sup>4</sup> /mol
O <sub>et</sub> ...O <sub>et</sub>	58298.9	0.24849	192.1	0.0
O <sub>et</sub> ...C	42931.6	0.27550	352.8	0.0
O <sub>et</sub> ...H	20432.6	0.24450	98.8	0.0
C...C	31615.1	0.30251	647.8	0.0
C...H	15046.7	0.27151	181.5	0.0
H...H	7161.2	0.24050	50.8	0.0
Al...Al	0.0	0.10000	0.0	0.0
Al...O <sub>Al</sub>	33652.8	0.29912	0.0	0.0
O <sub>Al</sub> ...O <sub>Al</sub>	524957.1	0.14900	530.4	0.0
O <sub>et</sub> ...Al	928077.6	0.24997	1139.9	0.0
O <sub>et</sub> ...O <sub>Al</sub>	951969.6	0.15784	239.7	0.0
C...Al	170201.1	0.30315	2160.9	0.0
C...O <sub>Al</sub>	1172167.0	0.24855	4537.0	0.0
H...Al	110177.8	0.26812	669.5	0.0
H...O <sub>Al</sub>	998796.7	0.19945	919.0	0.0
Li...Li	44195.0	0.13742	0.0	9.3
Li...O <sub>et</sub>	191106.0	0.17510	0.0	76.9
Li...C	8140.0	0.37994	0.0	473.2
Li...H	13139.0	0.22852	0.0	77.4
Li...Al	1415454.0	0.09091	3.5	0.0
Li...O <sub>Al</sub>	5744045.0	0.15038	1155.6	0.0
B...B	0.0	0.10000	0.0	0.0
B...O <sub>et</sub>	0.0	0.10000	0.0	0.0
B...C	0.0	0.10000	0.0	0.0
B...H	0.0	0.10000	0.0	0.0
B...Al	0.0	0.10000	0.0	0.0
B...O <sub>Al</sub>	0.0	0.10000	0.0	0.0
Li...B	0.0	0.10000	0.0	0.0
F...F	1295087.0	0.13990	65.9	0.0
F...O <sub>et</sub>	4530495.0	0.15616	49.1	0.0
F...C	2509348.0	0.17017	56.5	0.0
F...H	453450.4	0.16385	40.7	0.0
F...Al	8843424.0	0.20262	3023.4	0.0
F...O <sub>Al</sub>	9833345.0	0.15373	264.0	0.0
Li...F	1148106.7	0.12752	45.1	0.0
F...B	0.0	0.10000	0.0	0.0

An additional (so-called “slab”) model was created to simulate the interface between the polymer electrolyte and a larger nanoparticle. A slab of  $3 \times 3 \times 5$   $\alpha$ - $\text{Al}_2\text{O}_3$  unit cells was arranged at the bottom of a hexagonal simulation box. The slab was also “computer annealed” at 2000 K to relax its surface. The rest of the simulation box was then filled with the amorphous PEO– $\text{LiBF}_4$  system with Li/EO ratio 1:20.

A total of three systems were simulated:

- A rectangular “particle-free” simulation box ( $24 \times 24 \times 24$  Å) containing  $\text{LiBF}_4$  and an amorphous PEO chain of 200 EO monomers.
- A cubic “particle” simulation box ( $31 \times 31 \times 31$  Å) containing salt, particle, and an amorphous PEO chain of 455 EO monomers.
- A “slab” model ( $14.25 \times 12.35 \times 200$  Å; hexagonal setting) containing randomly inserted salt ions,  $\alpha$ - $\text{Al}_2\text{O}_3$  slab and an amorphous PEO chain of 294 EO monomers.

### 3. The simulation method

Molecular Dynamics (MD) simulation involves the simultaneous solution of Newton’s equations of

motion for all atoms (or ions) in an appropriately chosen simulation box. A local version of DL\_POLY with force fields developed earlier for PEO [13],  $\beta'$ -alumina [14], and  $\text{LiBF}_4$  [10,15,16] was used. Parameters in the Buckingham potential:

$$U(r) = A \exp\left(-\frac{B}{r}\right) - \frac{C}{r^6} - \frac{D}{r^4} + \frac{q_1 q_2}{4\pi\epsilon_0 r}$$

are listed in Table 1.

The middle layer of the  $\alpha$ - $\text{Al}_2\text{O}_3$  slab was kept tethered in the simulation box to represent the “bulk” of the large nanoparticle. Harmonic tethering potential ( $U(r) = kr^2/2$ ) was used with force constant  $k = 652.0$  kcal/(mol Å<sup>2</sup>) for  $\text{Al}_t$  and  $k = 545.4$  kcal/(mol Å<sup>2</sup>) for  $\text{O}_t$  [17] ( $\text{Al}_t$ : tethered Al in the slab,  $\text{O}_t$ : tethered oxygen in the slab).

The MD simulations use periodic boundary conditions and an Ewald summation to calculate the electrostatic forces at longer distances. Each simulation consists of an equilibration period of 50 ps followed by NVT simulation for 100 ps, followed by NpT simulation (Nose–Hoover model) for 1000 ps at nominal temperature 293 K. Sampling was made every 1 ps (every 1000 time-steps) in the simulation. Models

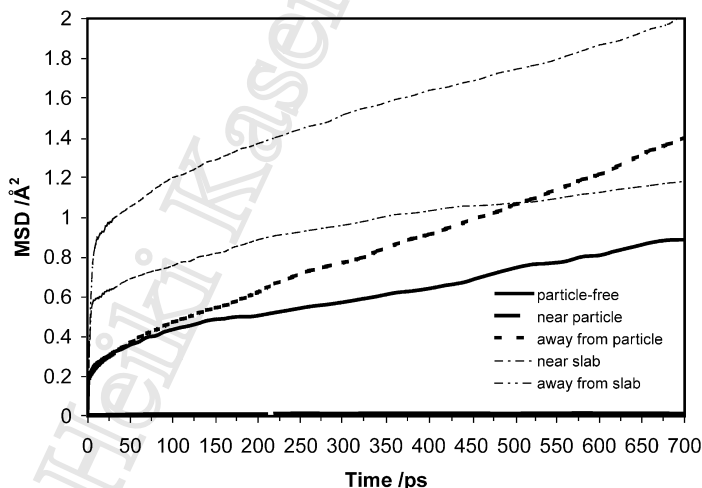


Fig. 1. Mean-square displacement (MSD) for  $\text{Li}^+$  for  $\text{LiBF}_4(\text{PEO})_{20}$  (particle-free);  $14$  Å diameter  $\text{Al}_2\text{O}_3$  particle in  $\text{LiBF}_4(\text{PEO})_{20}$ ; and  $\alpha$ - $\text{Al}_2\text{O}_3$  slab in  $\text{LiBF}_4(\text{PEO})_{20}$ .

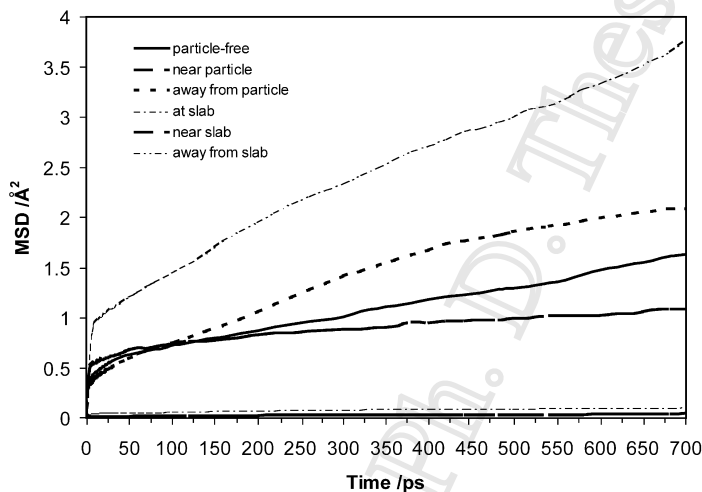


Fig. 2. MSD for  $B^-$  for  $LiBF_4(PEO)_{20}$  (particle-free); 14 Å diameter  $Al_2O_3$  particle in  $LiBF_4(PEO)_{20}$ ; and  $\alpha-Al_2O_3$  slab in  $LiBF_4(PEO)_{20}$ .

were prepared on a local array of PCs. This research was conducted using the resources of the High Performance Computing Centre North (HPC2N) and our local PC-Wulfkit cluster.

#### 4. Results and discussion

The space around the particle was divided into the regions called “near particle” (0–4 Å from the

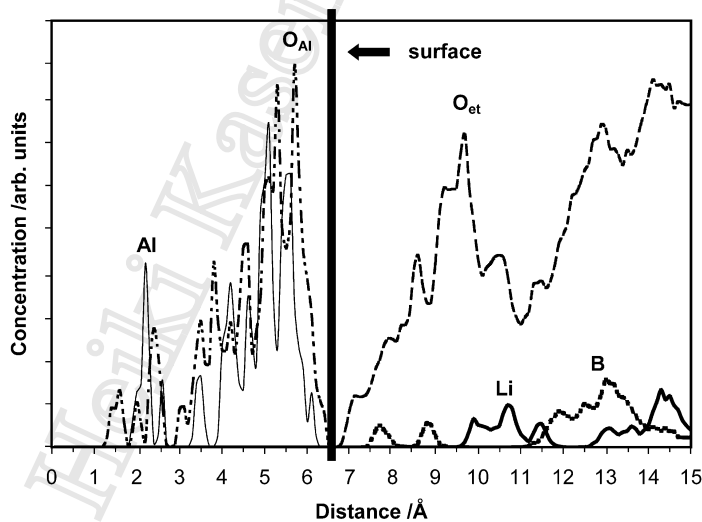


Fig. 3. Atom density distribution for the 14 Å diameter  $Al_2O_3$  particle in  $LiBF_4(PEO)_{20}$ .



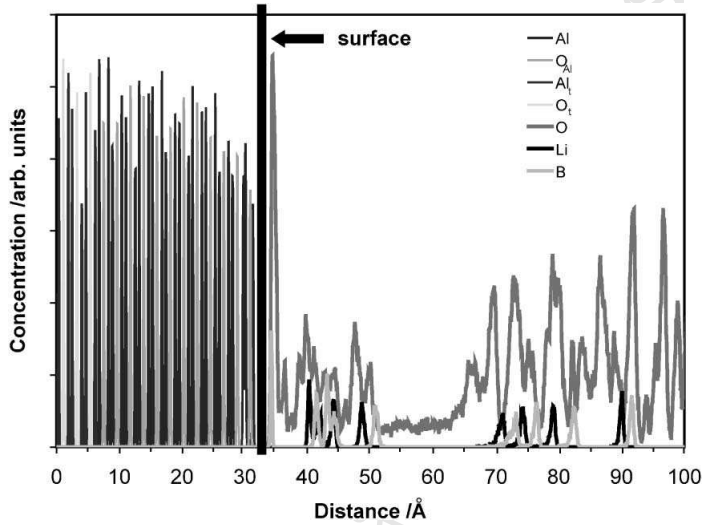


Fig. 4. Atom density distribution for the  $\alpha$ - $\text{Al}_2\text{O}_3$  slab in  $\text{LiBF}_4(\text{PEO})_{20}$ .

particle surface) and “away from particle” ( $>4 \text{ \AA}$  from the particle surface). The PEO sheet in the “slab” model was divided into zones parallel to the  $\text{Al}_2\text{O}_3$  surface: 0–5  $\text{\AA}$  (“at slab”), 5–20  $\text{\AA}$  (“near slab”), and  $>20 \text{ \AA}$  from the slab surface (“away from slab”).

Since our goal is to study the influence of the nanoparticles on the structure and dynamical proper-

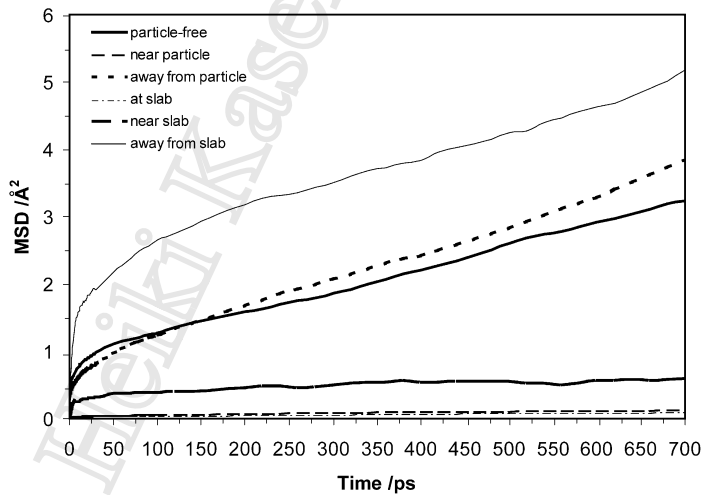


Fig. 5. MSD for  $\text{O}_{ca}$  for  $\text{LiBF}_4(\text{PEO})_{20}$  (particle-free); 14  $\text{\AA}$  diameter  $\text{Al}_2\text{O}_3$  particle in  $\text{LiBF}_4(\text{PEO})_{20}$ ; and  $\alpha$ - $\text{Al}_2\text{O}_3$  slab in  $\text{LiBF}_4(\text{PEO})_{20}$ .

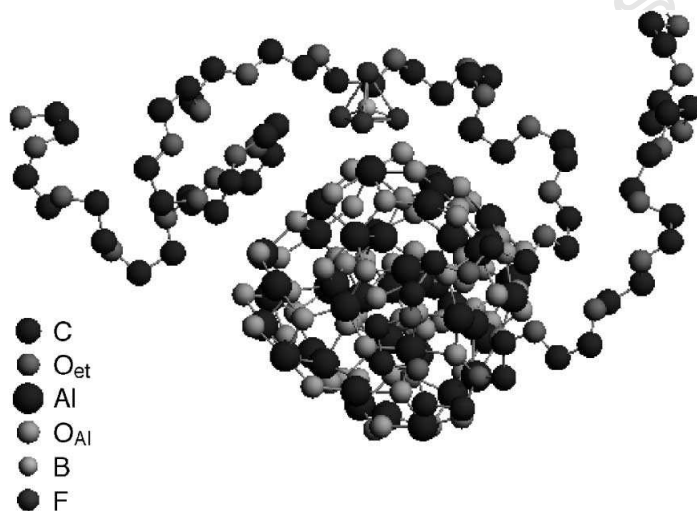


Fig. 6. Local structure around the anion bound to the nanoparticle.

ties of the polymer–salt system, let us first look at the mobility of the  $\text{Li}^+$  ion as the most interesting lithium-polymer battery related feature.

We see the first and one of the most important effects of the nanoparticle in Fig. 1: the slope of the Mean-Square Displacement (MSD) plot for  $\text{Li}^+$  ions

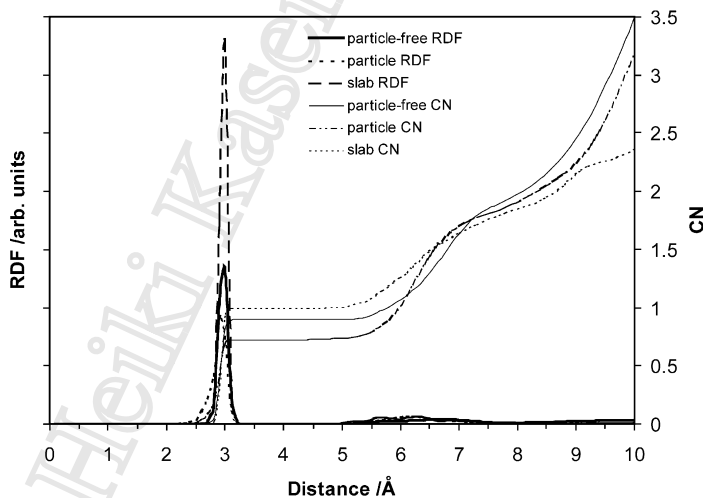


Fig. 7. Radial distribution function (RDF) and coordination number (CN) for Li–B for  $\text{LiBF}_4(\text{PEO})_{20}$  (particle-free); 14 Å diameter  $\text{Al}_2\text{O}_3$  particle in  $\text{LiBF}_4(\text{PEO})_{20}$ ; and  $\alpha\text{-Al}_2\text{O}_3$  slab in  $\text{LiBF}_4(\text{PEO})_{20}$ .

“away from particle” (directly proportional to Li-ion self-diffusion constant and conductivity) is at least twice as large as in the system without nanoparticles. The ion conductivity clearly increases on adding the nanoparticle. Note that  $\text{Li}^+$  ion concentration is the same in both systems (1:20).

The effect is not as large in the “slab” system (Fig. 1); there is very little difference in the slopes of the MSD curves for  $\text{Li}^+$  ions in the “away from slab” region and in the “particle-free” system.

The anion mobility away from the particle surface is comparable to that in the “particle-free” system as seen in Fig. 2. Away from the slab surface, the slope of the MSD curve is greater than in the “particle-free” system.

Closer to the particle surface, we see (Fig. 1) that the mobility of  $\text{Li}^+$  ions decreases greatly. It is remarkable that  $\text{Li}^+$  ions show no mobility in the region  $< 5$

Å from the  $\alpha\text{-Al}_2\text{O}_3$  slab surface (Fig. 1) and in the “near slab” region, the mobility of  $\text{Li}^+$  ions is low.

Almost the same applies to the anion mobility: near the particle surface, the mobility is very low (Fig. 2). There is still a slight mobility in the region  $< 5$  Å from the slab surface, where  $\text{Li}^+$  ions have no mobility at all. Anion mobility is smaller in the “near slab” region than in the “particle-free” system.

A second important observation is that  $\text{Li}^+$  ions are not found near the particle surface; they all stay outside the immobilised PEO “coordination sphere” around the nanoparticle. Fig. 3 shows this very low  $\text{Li}^+$ -ion concentration near the particle surface. At the same time, the  $\text{BF}_4^-$  ion concentration is higher than the  $\text{Li}^+$  ion concentration near the particle surface.

The atomic density distribution plot for the “slab” system (Fig. 4) shows the presence of anions at the

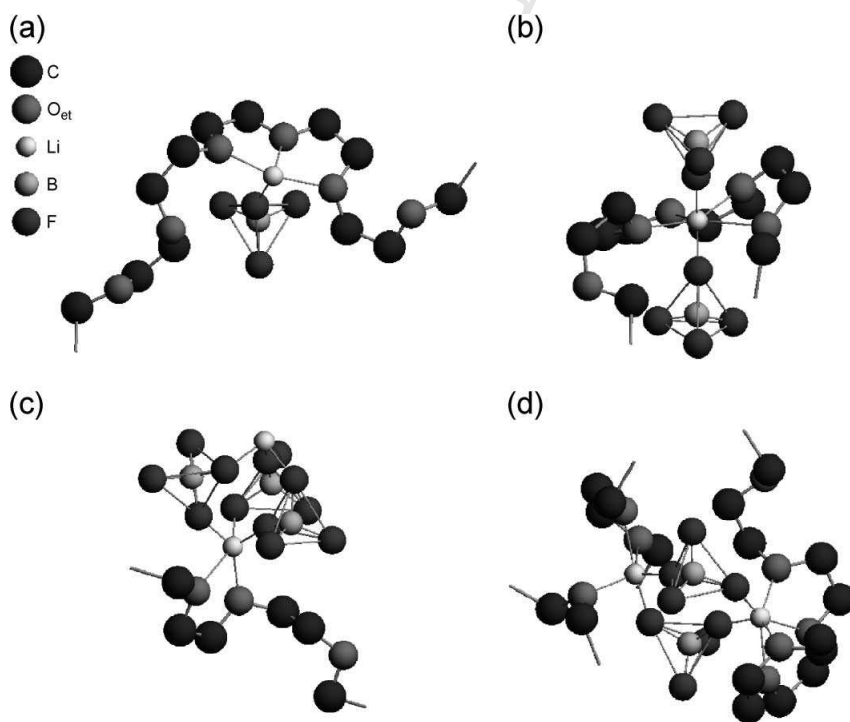


Fig. 8. Local structures of ion pairs and ion clusters: (a) ion pair in  $\text{LiBF}_4(\text{PEO})_{20}$  (charge: 0); (b) ion cluster in  $\text{LiBF}_4(\text{PEO})_{20}$  (charge: 0); (c) ion-cluster in 14 Å  $\text{Al}_2\text{O}_3$  particle- $\text{LiBF}_4(\text{PEO})_{20}$  system (charge: -1); (d) ion-cluster in  $\alpha\text{-Al}_2\text{O}_3$  slab- $\text{LiBF}_4(\text{PEO})_{20}$  system.

slab surface, but with no  $\text{Li}^+$  ions in the same region. The first  $\text{Li}^+$  ions appear ca. 8 Å from the slab surface along with anions; no ions are then found 20–35 Å from the slab surface. The rest of the salt ions are in the “away from particle” region.

The third observed effect of adding a particle is that the PEO chain forms a “coordination sphere” around the nanoparticle (Fig. 3). This does not involve a continuous section of chain, but rather successive chain segments at different points along its length, each containing four to five EO monomers. In the “slab” system, PEO forms a 20-Å-thick layer near the slab surface, followed by a 15-Å-thick layer of low-concentration PEO (Fig. 4). The PEO concentration then increases again.

The MSD plot for the ether oxygens (Fig. 5) shows that this “coordination sphere” around the particle is highly immobile. Away from the particle, the ether-oxygen mobility increases to a level slightly higher than in the “particle-free” system. The layer near the slab surface is similarly immobilised in the “slab” system. In regions away from the slab surface, the ether-oxygen mobility is roughly the same as in the “particle-free” system.

The structural effects on the PEO–salt system of adding the nanoparticle or the alumina slab are

intimately related to the effects seen for Li-ion mobility. The most interesting is the formation of the immobilised PEO sphere around the nanoparticle. It must be stressed that this sphere is a direct effect of the nanoparticle, not simply a trivial result of the polymer being forced away from the inserted particle. On the contrary, the chain was generated to fill the space around the particle. As seen from the atom density plot, the sphere immobilises two to three anions, releasing “free” Li ions into the outlying PEO (Fig. 6).

A similar effect is seen in the “slab” system, where one to two anions bind to the slab surface. Although we find no  $\text{Li}^+$  ions at the slab surface, they exist in this immobilised “near slab” region.

The mobility of  $\text{Li}^+$  ions is higher away from the particle and slab surfaces than in “particle-free” system despite ion-clustering effect between  $\text{Li}^+$  and  $\text{BF}_4^-$  ions. This cluster formation is clearly seen in Fig. 7, where the Li–B coordination number is the highest for the “slab” system and lowest for the “particle” system. Up to 70% of  $\text{Li}^+$  ions are involved in cluster formation in the “particle-free” system; up to 60% in the “particle” system, and up to 87% in the “slab” system. These percentages include  $\text{Li}^+$  ions occurring both in  $\text{Li}^+ \dots \text{BF}_4^-$  pairs

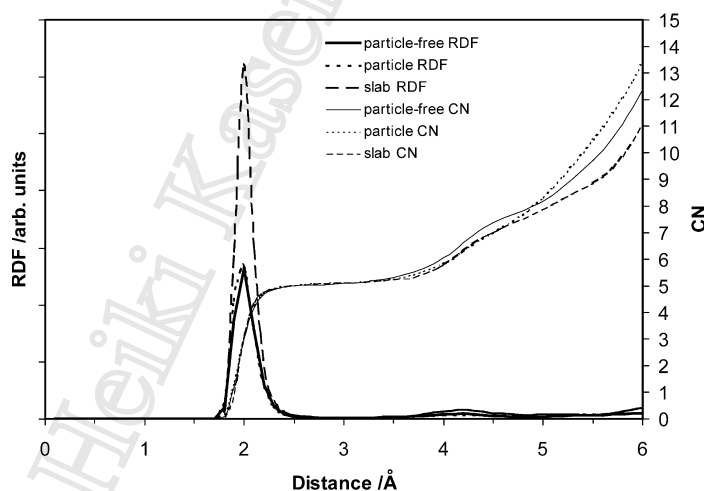


Fig. 9. RDF and CN for  $\text{Li}-\text{O}_{\text{et}}$  for  $\text{LiBF}_4(\text{PEO})_{20}$  (particle-free); 14 Å diameter  $\text{Al}_2\text{O}_3$  particle in  $\text{LiBF}_4(\text{PEO})_{20}$ ; and  $\alpha\text{-Al}_2\text{O}_3$  slab in  $\text{LiBF}_4(\text{PEO})_{20}$ .

(Fig. 8a) and in larger ion clusters. In the “particle-free” system, two complexes were found comprising two anions and one Li ion (Fig. 8b). These are the same complex as found in the “particle” system, where we also find a complex of three anions and two Li<sup>+</sup> ions (Fig. 8c). The slab system contains only one complex comprising two anions and two Li<sup>+</sup> ions (Fig. 8d).

We see from Fig. 9 that there are no significant differences in the Li...O coordination between the different systems.

## 5. Conclusions

The results presented here constitute the first simulation evidence of the effect of adding inorganic nanosized fillers on the mobility of Li ions in a polymer host.

The enhancement of Li<sup>+</sup>-ion mobility away from the particle surface and, to a lesser extent, away from the slab surface compared to Li<sup>+</sup>-ion mobility in the “particle-free” system is a result of structural changes in the PEO–salt system on adding the particle or slab. The formation of the immobilised “coordination sphere” around the particle and the immobilised layer near the slab surface can be seen as the most important single factor influencing ion mobility. The immobilised chain binds a fraction of the anions to the particle and slab surfaces, resulting in an excess of Li<sup>+</sup> ions in the regions away from these surfaces.

Ion pairing and clustering also occur in the regions away from the surfaces for all systems, but is largest for the “slab” system and smallest for the “particle” system, where Li<sup>+</sup>-ions exhibit at least twice as high a mobility away from the particle surface as in the “particle-free” system. Since ion clustering is less in the “particle” system than in the “particle-free” system, we can conclude that the nanoparticle serves to dissociate the LiBF<sub>4</sub> salt. This effect is not so clear in the “slab” system, where the mobility of Li<sup>+</sup> ions is only slightly higher than in “particle-free” system, but the ion clustering is larger.

## Acknowledgements

This work has been supported by grants from the Swedish Natural Science Research Council (NFR). Stipendia to Heiki Kasemägi from the Nordic Energy Research Programme (NEFP), the Kami Research Foundation (KFS), and the Estonian Science Foundation (ETF) grant no. 4513 are all gratefully acknowledged, as is the fine service provided by the High Performance Computing Centre North (HPC2N) in Sweden.

## References

- [1] F.M. Gray, *Polymer Electrolytes*, The Royal Society of Chemistry, Cambridge, 1997.
- [2] S. Chintapalli, R. Fresh, *Solid State Ionics* 86–88 (1996) 341.
- [3] L.R.A.K. Bandara, M.A.K.L. Dissanayake, B.-E. Mellander, *Electrochim. Acta* 43 (1998) 1447.
- [4] C. Capiglia, P. Mustarelli, E. Quartarone, C. Tomasi, A. Magistris, *Solid State Ionics* 118 (1999) 73.
- [5] F. Croce, G.B. Appetecchi, L. Persi, B. Serosati, *Nature* 394 (1998) 456.
- [6] A.S. Best, A. Ferry, D.R. MacFarlane, M. Forsyth, *Solid State Ionics* 126 (1999) 269.
- [7] W. Krawiec, L.G. Scanlon Jr., J.P. Fellner, R.A. Vaia, S. Vasudevan, E.P. Giannelis, *J. Power Sources* 54 (1995) 310.
- [8] F. Croce, L. Persi, F. Ronci, B. Scrosat, *Solid State Ionics* 135 (2000) 47.
- [9] F. Müller-Plathe, W.F. van Gunsteren, *J. Chem. Phys.* 103 (1995) 4745.
- [10] J.-S. Soetens, C. Millot, B. Maignet, *J. Phys. Chem. A* 102 (1998) 1055.
- [11] *International Tables for Crystallography*. Vol. A Space-Group Symmetry, ed. T. Hahn, 4th revised edition (1996).
- [12] T.C. Huang, W. Parrish, N. Masciocchi, P.W. Wang, *Adv. X-Ray Anal.* 33 (1990) 295.
- [13] S. Neyertz, D. Brown, J.O. Thomas, *J. Chem. Phys.* 101 (1994) 10064.
- [14] S. Edvardsson, M. Klintonberg, J.O. Thomas, *Phys. Rev. B* 54 (1996) 17476.
- [15] A.K. Rappe, C.J. Casewit, K.S. Colwell, W.A. Goddard III, W.M. Skiff, *J. Am. Chem. Soc.* 114 (1992) 10024.
- [16] G.D. Smith, R.L. Jaffe, H. Partridge, *J. Phys. Chem. A* 101 (1997) 1705.
- [17] T. Pilati, F. Demartin, C.M. Gramaccioni, *Acta Crystallogr., Sect. A* 49 (1993) 473.

# III

*Heiki Kasemagi Ph. D. Thesis*



PERGAMON

Available online at www.sciencedirect.com

SCIENCE @ DIRECT®

ELECTROCHIMICA  
Acta

Electrochimica Acta 00 (2003) 1–6

www.elsevier.com/locate/electacta

# Molecular dynamics simulation of temperature and concentration dependence of the ‘filler’ effect for the LiCl/PEO/Al<sub>2</sub>O<sub>3</sub>-nanoparticle system

Heiki Kasemägi<sup>a,b</sup>, Mattias Klintenberg<sup>c</sup>, Alvo Aabloo<sup>d</sup>, John O. Thomas<sup>b,\*</sup><sup>a</sup> Institute of Materials Science, Department of Physics, Tartu University, Tähe 4, 51010 Tartu, Estonia<sup>b</sup> Materials Chemistry, Ångström Laboratory, Uppsala University, Box 538, SE-751 21 Uppsala, Sweden<sup>c</sup> Condensed Matter Theory Group, Department of Physics, Uppsala University, Box 530, SE-751 21 Uppsala, Sweden<sup>d</sup> Institute of Physics, Tartu University, Tähe 4, 51010 Tartu, Estonia

Received 19 May 2002; accepted 17 October 2002

## Abstract

A system involving amorphous LiCl(PEO)<sub>x</sub> for  $x = 20, 35$  and  $50$ , and a  $14 \text{ \AA}$  diameter Al<sub>2</sub>O<sub>3</sub> ‘filler’ particle has been simulated at nominal temperatures  $290$  and  $330 \text{ K}$  by the molecular dynamics method. The mobility of Li-ions is found to increase on the addition of the nanoparticle at  $330 \text{ K}$  and Li:EO ratio  $1:50$ , but decreases or remains unchanged at other temperatures and concentrations. Lower temperature and concentration are generally associated with a lower Li–Cl coordination number and a correspondingly higher number of unpaired/unclustered ions in the system. A number of free Li<sup>+</sup> ions and some Li–Cl pairs/clusters are found in an immobilised poly(ethylene oxide) (PEO) ‘coordination sphere’ around the nanoparticle. This reduces the number of Li<sup>+</sup> ions in regions away from the particle surface. The number of ‘free’ Li<sup>+</sup> ions away from the particle surface is largest for the intermediate composition  $x = 35$  and at  $290 \text{ K}$  ( $\sim 23\%$  of the total number of lithium ions in the system); smaller for  $x = 50$  ( $\sim 11\%$  at both temperatures), and even smaller at  $x = 20$  ( $\sim 5\%$  at  $290 \text{ K}$  and  $\sim 9\%$  at  $330 \text{ K}$ ).

© 2003 Published by Elsevier Science Ltd.

**Keywords:** Molecular dynamic method; Filler; Poly(ethylene oxide)

## 1. Introduction

The rechargeable lithium-ion battery has now become a popular power source for many applications; typically mobile phones, laptop computers and other small-sized electronic equipment. The development of even safer lithium-ion polymer batteries has been a general goal for many years. Poly(ethylene oxide) (PEO) is often seen as the prototype polymer electrolyte host material for battery concepts. At ambient temperature, PEO has quite a poor lithium-ion conductivity as a result of its high degree of crystallinity [1]; higher values can be achieved around  $60\text{--}80 \text{ }^\circ\text{C}$  [1,2]. However, recent experimental work has shown that some crystalline PEO–

lithium salt systems have a potentially higher ionic conductivity than their amorphous counterparts [3].

Our interest here is concentrated on the effect of nanosized inorganic ‘plasticiser’ particles on the conductivity of amorphous LiX/PEO. There is much experimental evidence to show improved conductivity on adding nanoparticles of different types and sizes to the PEO–lithium salt system [2,4–11].

We have earlier made a number of computer simulations of PEO–lithium salt systems [12–16]. Recent molecular dynamics (MD) simulations of the PEO/LiBF<sub>4</sub>/Al<sub>2</sub>O<sub>3</sub>-nanoparticle system [17] have confirmed the available experimental evidence for increased Li-ion mobility on the addition of nanosized inorganic particles to the amorphous PEO–lithium salt system. Our earlier simulations involving PEO/lithium-salt/nanoparticle systems with monoatomic anions like Cl<sup>−</sup>, Br<sup>−</sup> and I<sup>−</sup> [18] showed significant levels of outsalting and reduced Li-ion mobility at higher temperature and salt

\* Corresponding author. Tel.: +46-18-513548.

E-mail address: josh.thomas@mkem.uu.se (J.O. Thomas).

concentrations. Since LiCl had earlier shown the least tendency to cluster, we chose to follow up this case in the present work. Moreover, potentials involving the  $I^-$  ions are difficult to derive reliably by quantum mechanics, making it more difficult to create a reliable force field for LiI. Also, Müller-Plathe and van Gunsteren [19] have already shown a mechanism for ion-pair formation in the LiI–PEO system.

We wish to suppress salt clustering and crystallization effects in the lithium-ion polymer battery. This makes it important to seek optimal conditions to avoid crystallization. Also, in a more general sense, phase-separation phenomena are important, not least in a biological context. This present work can thus be seen as an extension to our earlier work on nanoparticles in  $LiX(PEO)_{20}$  for  $X = Br, Cl$  and  $I$  [18]. We have used MD simulation to study the temperature and salt-concentration dependence of the effect of ‘nano-fillers’ on the PEO/LiCl/ $Al_2O_3$  system. We here choose a lithium salt which had earlier shown the least tendency to cluster (LiCl), a single particle-size (14 Å), lower temperatures (290 and 330 K) and concentrations (Li:EO ratios of 1:20, 1:35 and 1:50).

## 2. The model

A charge-neutral fragment of  $\alpha-Al_2O_3$  (corundum) was extracted from its rhombohedral crystal structure: space-group  $R3c$  (No. 167) [20]; unit-cell parameters:  $a = 4.75$  Å,  $c = 12.99$  Å (hexagonal setting) [21]. The particle was then ‘computer-annealed’ at 2000 K to give it a roughly spherical form (diameter 14 Å; 115 atoms) with predominantly oxygen atoms at its surface.

Two systems were simulated:

- A ‘particle-free’ simulation box ( $27.9 \times 22.3 \times 23.5$  Å) containing  $Li^+$  and  $Cl^-$  ions and an amorphous PEO chain of 200 EO monomers; effectively,  $LiCl(PEO)_x$  for  $x = 20, 35$  and  $50$ .
- A cubic simulation box ( $33.0 \times 33.0 \times 33.0$  Å) containing  $Li^+$  and  $Cl^-$  ions and an amorphous PEO chain of 455 EO monomers; effectively,  $LiCl(PEO)_x$  for  $x = 20, 35$  and  $50$ , but with the addition of a approximately 14 Å diameter  $Al_2O_3$  particle.

The particle represents  $\sim 10\%$  of the total mass and  $\sim 6\%$  of the total simulation-box volume. This also corresponds to a particle-area density of  $300 m^2/cm^3$  and to  $2.8 \times 10^{19}$  particles/cm<sup>3</sup>. The particle was placed at the centre of the cubic simulation box during system generation. The  $Li^+$  and  $Cl^-$  ions were then added randomly into both simulation boxes to give Li:EO ratios of 1:20, 1:35 and 1:50. The two simulation boxes were then filled with PEO: the chain was generated using pivotal Monte Carlo generation techniques to have as

low an energy as possible in the simulation box around the particle and/or salt ions. The salt ions were fixed during the chain generation process.

## 3. Simulation details

MD simulation involves the simultaneous solution of Newton’s equations of motion for all atoms (ions) in an appropriately chosen simulation box. A local version of DL\_POLY [22] was used with force fields developed earlier for PEO [12],  $\alpha$ -alumina [23], LiCl, Li–PEO and

Table 1

Potential parameters describing the long-range interactions in the systems  $LiCl(PEO)_x$  (particle-free) and with a 14 Å-diameter  $Al_2O_3$  particle for  $x = 20, 35$  and  $50$  ( $O_{Al}$ : particle oxygen;  $O_{et}$ : ether oxygen), where  $V(r) = A \exp(-B/r) - Cr^{-6} - Dr^{-8}$

Atom pair	$A$ (kcal mol <sup>-1</sup> )	$B$ (Å)	$C$ (kcal Å <sup>6</sup> mol <sup>-1</sup> )	$D$ (kcal Å <sup>4</sup> mol <sup>-1</sup> )
$O_{et} \cdots$	58298.9	0.24849	192.1	0.0
$O_{et}$				
$O_{et} \cdots C$	42931.6	0.27550	352.8	0.0
$O_{et} \cdots$	20432.6	0.24450	98.8	0.0
H				
$O_{et} \cdots$	928077.6	0.24997	1139.9	0.0
Al				
$O_{et} \cdots$	951969.6	0.15784	239.7	0.0
$O_{Al}$				
$C \cdots C$	31615.1	0.30251	647.8	0.0
$C \cdots H$	15046.7	0.27151	181.5	0.0
$C \cdots Al$	170201.1	0.30315	2160.9	0.0
$C \cdots$	1172167.0	0.24855	4537.0	0.0
$O_{Al}$				
$H \cdots H$	7161.2	0.24050	50.8	0.0
$H \cdots Al$	110177.8	0.26812	669.5	0.0
$H \cdots$	998796.7	0.19945	919.0	0.0
$O_{Al}$				
$Al \cdots Al$	0.0	0.10000	0.0	0.0
$Al \cdots$	33652.8	0.29912	0.0	0.0
$O_{Al}$				
$O_{Al} \cdots$	524957.1	0.14900	530.4	0.0
$O_{Al}$				
$Li \cdots$	191106.0	0.17510	0.0	76.9
$O_{et}$				
$Li \cdots C$	8140.0	0.37994	0.0	473.2
$Li \cdots H$	13139.0	0.22852	0.0	77.4
$Li \cdots Al$	53082940.0	0.14873	0.0	0.0
$Li \cdots$	62774060.0	0.11668	0.0	0.0
$O_{Al}$				
$Li \cdots Li$	44195.0	0.13742	0.0	9.3
$Li \cdots Cl$	30868.0	0.31797	0.0	729.4
$Cl \cdots$	40353.0	0.31056	1005.0	536.3
$O_{et}$				
$Cl \cdots C$	17926.0	0.36590	1273.3	67.2
$Cl \cdots H$	7543.0	0.32701	263.0	0.0
$Cl \cdots Al$	2633313.0	0.27671	14322.4	0.0
$Cl \cdots$	654978.0	0.23133	491.7	0.0
$O_{Al}$				
$Cl \cdots Cl$	70768.4	0.39622	29699.1	0.0



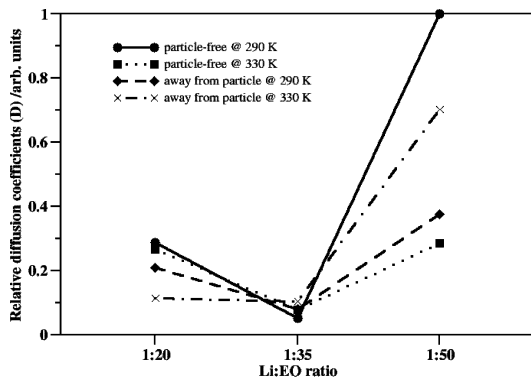


Fig. 1. Relative diffusion coefficients ( $D$ ) for  $\text{Li}^+$  in  $\text{LiCl}(\text{PEO})_x$  (particle-free) and  $> 4$  Å from a 14 Å diameter  $\text{Al}_2\text{O}_3$  particle in  $\text{LiCl}(\text{PEO})_x$ ;  $x = 20, 35$  and  $50$ .

119 Cl–PEO [24]. The parameters used in the Buckingham  
 120 potential are listed in the Table 1. The simulations use  
 121 periodic boundary conditions and an Ewald summation  
 122 to calculate the electrostatic forces at longer distances.  
 123 Each simulation consists of an equilibration period of 50  
 124 ps, followed by NVT (constant volume and tempera-  
 125 ture) simulation for 100 ps, and then NPT (constant  
 126 pressure and temperature) simulation (Nosé-Hoover  
 127 model) for upto 1000 ps. The system energy was  
 128 monitored during equilibration until the energy reached  
 129 a minimum. The simulation temperatures used were 290  
 130 and 330 K. Sampling was made every 1 ps (every 1000  
 131 time-steps) during the NpT simulation. The models were  
 132 prepared on local PC's and the final simulations made  
 133 using the resources of the High Performance Computing  
 134 Centre North (HPC2N), and our local PC-Wulfkit  
 135 cluster of 4 double-processor nodes.

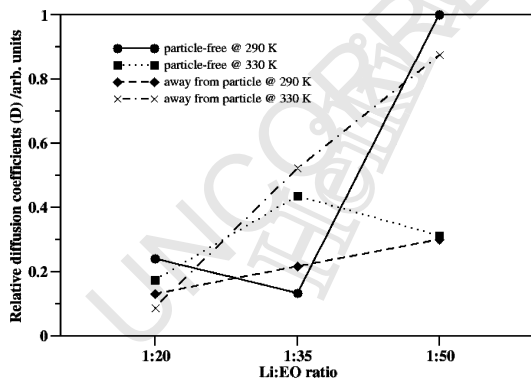


Fig. 2. Relative diffusion coefficients ( $D$ ) for  $\text{Cl}^-$  in  $\text{LiCl}(\text{PEO})_x$  (particle-free) and  $> 4$  Å from a 14 Å diameter  $\text{Al}_2\text{O}_3$  particle in  $\text{LiCl}(\text{PEO})_x$ ;  $x = 20, 35$  and  $50$ .

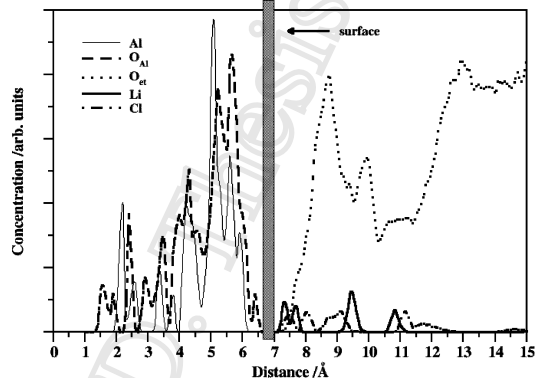


Fig. 3. Atom density distribution for the  $\text{Al}_2\text{O}_3$ – $\text{LiCl}(\text{PEO})_{35}$  system at 330 K.

#### 4. Results and discussion

136  
 137 For convenience, we refer to the region around the  
 138 particle as ‘near particle’ (0–4 Å from the particle  
 139 surface) and ‘away from the particle’ ( $> 4$  Å) from the  
 140 particle surface). The 290 K temperature is referred to as  
 141 the ‘lower’, and 330 K as the ‘higher’ temperature;  
 142 similarly, the 1:20 concentration as ‘higher’, 1:35 as  
 143 ‘intermediate’, and 1:50 as ‘lower’ concentration.

##### 4.1. Ion mobility

144  
 145 Let us first probe the concentration and temperature  
 146 dependence of the effect of the nanoparticle on the  
 147 mean-square-displacement (MSD) of the  $\text{Li}^+$  ions. In  
 148 the ‘near particle’ region, the  $\text{Li}^+$  MSD is at least an  
 149 order of magnitude lower than in the region ‘away from  
 150 the particle’. This effect is also maintained for the  $\text{Cl}^-$   
 151 ions and the ether oxygens at all concentrations and  
 152 temperatures studied. Fig. 1 shows  $\text{Li}^+$  ion mobilities at  
 153 different temperatures and concentrations in the region  
 154  $> 4$  Å away from the particle surface compared to that  
 155 in the particle-free system. At the higher concentration,  
 156 the  $\text{Li}^+$  ion mobility becomes slightly smaller away  
 157 from the particle on the addition of the nanoparticle at  
 158 both temperatures. This effect is greater at 330 K, where  
 159 the mobility is only half that in the particle-free system.  
 160 Interestingly, such effects disappear at the intermediate  
 161 concentration, where mobilities are only approximately  
 162 25% (perhaps insignificantly) higher away from the  
 163 particle than in the particle-free system; moreover, the  
 164 lithium-ion mobility at 330 K is identical away from the  
 165 particle to that at the higher concentration, while a clear  
 166 increase occurs as we decrease the concentration further  
 167 (to  $x = 50$ ). Notably, the mobility in the particle-free  
 168 system is only 40% of that away from the particle at this  
 169 concentration, while the opposite effect is seen at 290 K.  
 170 The most noticeable overall effect is that (at all  
 171

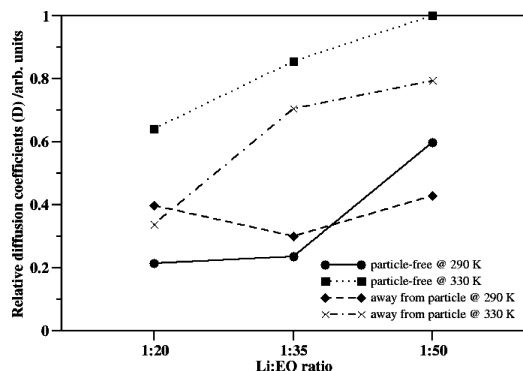


Fig. 4. Relative diffusion coefficients ( $D$ ) for ether O's in  $\text{LiCl}(\text{PEO})_x$  (particle-free) and  $> 4 \text{ \AA}$  from a  $14 \text{ \AA}$  diameter  $\text{Al}_2\text{O}_3$  particle in  $\text{LiCl}(\text{PEO})_x$ ;  $x = 20, 35$  and  $50$ .

171 temperatures) the  $\text{Li}^+$  ion mobility passes through a  
 172 minimum at the intermediate concentration. There is,  
 173 indeed, clear experimental evidence [1,25] to show that  
 174  $\text{Li}^+$  ion conductivity passes through a minimum as a  
 175 function of salt concentration. Also, for a particle-free  
 176 system, Rietman et al. [26] show conductivity minima  
 177 for  $\text{LiBr}$  and  $\text{LiCl}$  in PEO on increasing the temperature.  
 178 Their results are in the same temperature range as our  
 179 simulations.

180 It is also interesting to examine the  $\text{Cl}^-$  mobility (Fig.  
 181 2): this follows the same general trends as seen in the  
 182  $\text{Li}^+$  mobility. One clear and perhaps significant differ-  
 183 ence, however, is that the  $\text{Cl}^-$  mobility only passes  
 184 through a minimum at the intermediate concentration in  
 185 the particle-free system at  $290 \text{ K}$ , but *increases linearly*  
 186 *away from the particle* with decreasing concentration at

187 both temperatures, with the largest difference compared  
 188 to the particle-free system occurring at  $x = 50$ .

#### 4.2. Polymer structure and dynamics

189  
 190 An immobilised PEO 'coordination sphere' is seen to  
 191 form around the particle upto approximately  $4 \text{ \AA}$  away  
 192 from the particle surface at all temperatures and  
 193 concentrations (Fig. 3). This same effect was seen earlier  
 194 for  $14$  and  $18 \text{ \AA}$  diameter  $\text{Al}_2\text{O}_3$  nanoparticles in the  
 195  $\text{LiCl}/\text{LiBr}/\text{Li}(\text{PEO})_{20}$  systems at  $360 \text{ K}$  [18]. It should be  
 196 stressed strongly that this effect is not a result of the  
 197 polymer simply being forced away from the inserted  
 198 particle; on the contrary, the polymer was generated so  
 199 as to fill the space left in the simulation box around the  
 200 particle. The mobility of ether oxygens ( $\text{O}_{\text{et}}$ 's) (Fig. 4)  
 201 is lower in regions away from the particle compared to the  
 202 particle-free case for all concentrations at  $330 \text{ K}$ —by  
 203 approximately  $50\%$  at  $x = 20$  and by  $20\%$  at lower  
 204 concentrations. In contrast, at  $290 \text{ K}$ , the  $\text{O}_{\text{et}}$  mobility  
 205 increases by approximately  $50\%$  for  $x = 20$  and by  
 206 approximately  $20\%$  for  $x = 35$ ; it then decreases by  
 207 approximately  $30\%$  for  $x = 50$ .

#### 4.3. Ion-pairing/clustering

208  
 209 We can note that the immobilised PEO chains in the  
 210 'near particle' region also host  $\text{Li}^+$  and  $\text{Cl}^-$  ions; see  
 211 Fig. 3. In [18], some  $\text{Li}^+$  ions were found to bind to the  
 212 oxygens of the  $\text{Al}_2\text{O}_3$  particle surface. This is also seen  
 213 here (Fig. 5), along with a number of  $\text{Cl}^-$  ions. Even  
 214  $\text{Li}^+ - \text{Cl}^-$  ion-pairs are seen to occur in this region. The  
 215  $\text{Li}-\text{Cl}$  coordination numbers indicate that  $\text{Li}^+ - \text{Cl}^-$   
 216 pairs and smaller clusters form at all temperatures, both

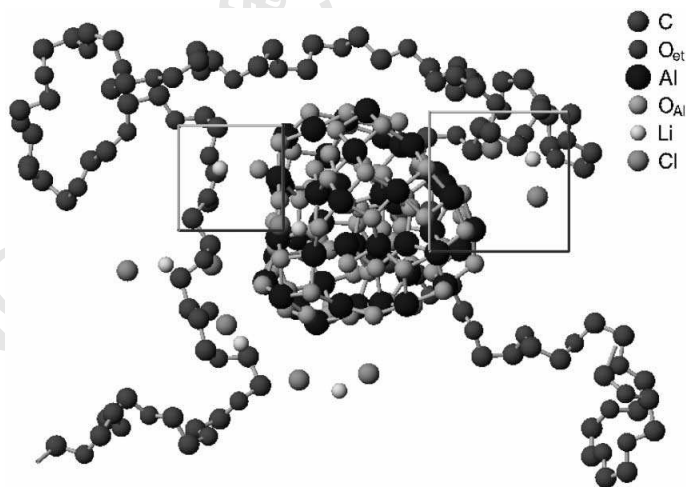


Fig. 5. A general view of a region near the  $\text{Al}_2\text{O}_3$  particle showing a 'free'  $\text{Li}^+$  ion linking PEO to the particle, and a  $[\text{LiCl}_2]^-$  cluster near the particle.

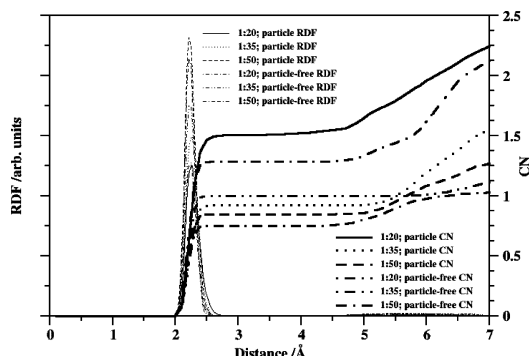


Fig. 6. Radial distribution function (RDF) and coordination number (CN) for  $\text{Li}^+ - \text{Cl}^-$  in  $\text{LiCl}(\text{PEO})_x$  (particle-free) and 14 Å diameter  $\text{Al}_2\text{O}_3$  particle in  $\text{LiCl}(\text{PEO})_x$  at 290K;  $x = 20, 35$  and  $50$ .

in the particle-free and in the nanoparticle-containing systems (Fig. 6);  $\text{Li}-\text{Cl}$  coordination numbers are  $\leq 1.5$  at 3.5 Å in all systems and at all temperatures and concentrations. At 330 K, the  $\text{Li}^+ - \text{Cl}^-$  coordination number increases from 1.2 to 1.4 on the addition of the particle at the higher concentrations, but again falls from 1.3 to 1.2 at the intermediate, and from 1.5 to 0.9 at lower concentrations. At 290 K, a lower  $\text{Li}^+ - \text{Cl}^-$  coordination number is seen in the particle system than in the particle-free system (from 1.0 vs. 0.9) only at intermediate concentration. The coordination number increases from 1.3 to 1.5 and from 0.75 to 0.85, respectively, at the higher and lower concentrations.

All this combines to suggest highly sensitive ion-clustering effects—both with respect to temperature and ion concentration. This is summarized in Fig. 7 in terms of the percentage of ‘free’  $\text{Li}^+$  ions in different situations; this number is seen generally to increase on the addition of the nanoparticle. The effect is stronger at lower concentrations and higher temperatures, but at

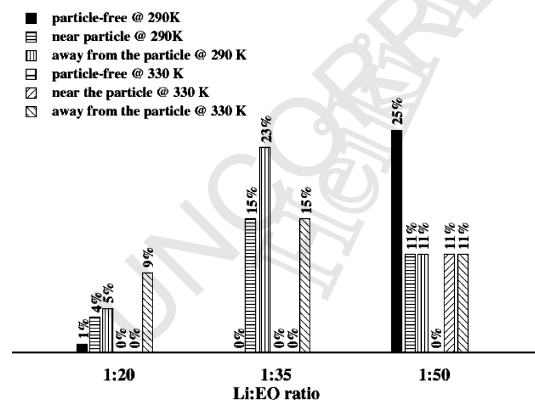


Fig. 7. Histogram of ‘free’  $\text{Li}^+$  ions in  $\text{LiCl}(\text{PEO})_x$  (particle-free) and 14 Å diameter  $\text{Al}_2\text{O}_3$  particle in  $\text{LiCl}(\text{PEO})_x$ ;  $x = 20, 35$  and  $50$ .

$x = 50$  and at 290 K, a slightly opposite effect is seen on the addition of the particle. It can be that, at higher salt concentrations,  $\text{Li}^+$  ions form more ion-pairs/clusters since they have access to and hence more opportunity to form bond with a larger number of  $\text{Cl}^-$  ions. At the lowest concentration studied (1:50), the number of  $\text{Cl}^-$  ions around  $\text{Li}^+$  ions is lower, resulting in more ‘free’  $\text{Li}^+$  ions.

It is seen from Table 2 that the  $\text{Li}-\text{O}_{\text{et}}$  coordination number increases on the addition of the particle only for  $x = 50$  and at 330 K, but decreases in all other cases. In the ‘particle’ system, the  $\text{Li}-\text{O}_{\text{et}}$  coordination number shows clear concentration dependence, increasing as we lower the concentration.

## 5. A general comment

While it is difficult from the above set of observations to discern any simple overriding trends, one thing is very clear: our simulations demonstrate highly sensitive temperature and concentration dependence in the effect on ion-pairing/clustering phenomena of the introduction of small nanoparticles into a polymer electrolyte. Implicitly, such phenomena will have a decisive influence on lithium-ion transport and consequently on battery performance.

## Acknowledgements

This work has been supported by grants from the Swedish Research Council (VR) and the Estonian Science Foundation (ETF; grant no. 4513). Stipendia to Heiki Kasemägi from the Nordic Energy Research (NEFP) and the Kami Research Foundation (KFS) are all gratefully acknowledged, as is the fine service provided by the High Performance Computing Centre North (HPC2N) and the Parallel Computer Center (PDC) at KTH in Sweden.

Table 2

Coordination number for  $\text{Li}-\text{O}_{\text{et}}$  in  $\text{LiCl}(\text{PEO})_x$  (particle-free) and with a 14 Å-diameter  $\text{Al}_2\text{O}_3$  particle for  $x = 20, 35$  and  $50$  ( $\text{O}_{\text{et}}$ : ether oxygen)

Concentration	290 K		330 K	
	Free	Particle	Free	Particle
1:20	4.6	4.0	4.7	4.3
1:35	5.3	4.6	4.8	4.3
1:50	5.3	5.1	4.6	5.0

271 **References**

- 272 [1] F.M. Gray, *Polymer Electrolytes*, The Royal Society of Chem-  
273 istry, Cambridge, 1997.
- 274 [2] F. Croce, G.B. Appetecchi, L. Persi, B. Scrosati, *Nature* 394  
275 (1998) 456.
- 276 [3] Z. Gadjourova, Y.G. Andreev, D.P. Tunstall, P.G. Bruce, *Nature*  
277 412 (2001) 520.
- 278 [4] A.M. Sureshini, A.R. Kulkarni, A. Sharma, *Solid State Ionics*  
279 113–115 (1998) 179.
- 280 [5] S. Chintapalli, R. Frech, *Solid State Ionics* 86–88 (1996) 341.
- 281 [6] F. Croce, L. Persi, F. Ronci, B. Scrosati, *Solid State Ionics* 135  
282 (2000) 47.
- 283 [7] S.H. Sung, Y. Wang, L. Persi, F. Croce, S.G. Greenbaum, B.  
284 Scrosati, E. Plichta, *J. Power Sources* 97–98 (2001) 644.
- 285 [8] W. Krawiec, L.G. Scanlon, Jr., J.P. Fellner, R.A. Vaia, S.  
286 Vasudevan, E.P. Giannelis, *J. Power Sources* 54 (1995) 310.
- 287 [9] C. Capiglia, P. Mustarelli, E. Quartarone, C. Tomasi, A.  
288 Magistris, *Solid State Ionics* 118 (1999) 73.
- 289 [10] A.C. Bloise, C.C. Tambelli, R.W.A. Franco, J.P. Donoso, C.J.  
290 Magon, M.F. Souza, A.V. Rosario, E.C. Pereira, *Electrochim.*  
291 *Acta* 46 (2001) 1571.
- 292 [11] A.S. Best, A. Ferry, D.R. MacFarlane, M. Forsyth, *Solid State*  
293 *Ionics* 126 (1999) 269.
- 294 [12] S. Neyertz, D. Brown, J.O. Thomas, *J. Chem. Phys.* 101 (1994)  
295 10064.
- [13] S. Neyertz, D. Brown, J.O. Thomas, *Comput. Polym. Sci.* 5 296  
(1995) 107. 297
- [14] A. Aabloo, J.O. Thomas, *Comput. Theor. Polym. Sci.* 7 (1997) 47. 298
- [15] A. Aabloo, J.O. Thomas, *Electrochim. Acta* 43 (1998) 1361. 299
- [16] A. Aabloo, M. Klintonberg, J.O. Thomas, *Electrochim. Acta* 45 300  
(2000) 1425. 301
- [17] H. Kasemägi, M. Klintonberg, A. Aabloo, J.O. Thomas, *Solid*  
302 *State Ionics* 147 (2002) 367. 303
- [18] H. Kasemägi, M. Klintonberg, A. Aabloo, J.O. Thomas, *J. Mater.*  
304 *Chem.* 11 (2001) 3191. 305
- [19] F. Müller-Plathe, W.F. van Gunsteren, *J. Chem. Phys.* 103 (1995)  
306 4745. 307
- [20] T. Hahn (Ed.), *International Tables for Crystallography*. vol. A,  
308 fourth revised edition, 1996. 309
- [21] T.C. Huang, W. Parrish, N. Masciocchi, P.W. Wang, *Adv. X-ray*  
310 *Anal.* 33 (1990) 295. 311
- [22] The DL\_POLY Project, W. Smith, T. Forester, TCS Division,  
312 Daresbury Laboratory, Daresbury, Warrington WA4 4AD,  
313 England. 314
- [23] S. Edvardsson, M. Klintonberg, J.O. Thomas, *Phys. Rev. B* 54 315  
(1996) 17476. 316
- [24] G.D. Smith, R.L. Jaffe, H. Partridge, *J. Phys. Chem. A* 101 (1997)  
317 1705. 318
- [25] A. Magistris, P. Mustarelli, E. Quartarone, C. Tomasi, *Solid State*  
319 *Ionics* 136–137 (2000) 1241. 320
- [26] E.A. Rietman, M.L. Kaplan, R.J. Cava, *Solid State Ionics* 17 321  
(1985) 67. 322

# *Curriculum vitae*

## **Heiki Kasemägi**

Sünniaeg ja -koht: 11.11.1974, Tartu  
Kodakondsus: Eesti Vabariik  
Perekonnaseis: vallaline  
Aadress: Tartu Ülikooli Tehnoloogiainstituut  
Tähe 4 51010 Tartu Eesti  
Telefon: +372 5 118754, +372 7 375537  
Fax: +372 7 374 900  
E-mail: cipo@ut.ee

### **Haridus**

1997–1999 Tartu Ülikool, M. Sc. füüsika erialal  
1993–1997 Tartu Ülikool, B. Sc. füüsika erialal  
1982–1993 Tartu 7. Keskkool, kuldmedal

### **Teenistuskäik**

2003– Tartu Ülikool, Tehnoloogiainstituut, teadur  
1997–1999 Tartu Ülikool, Eksperimentaalfüüsika ja tehnoloogia  
instituut, vaneminsener  
1997 Tartu Ülikool, Eksperimentaalfüüsika ja tehnoloogia  
instituut, laborant

### **Teadustegevus**

Peamised uurimisvaldkonnad: **liitumioon-polümeeraku** materjalid — anorgaaniliste nano-osakeste mõju molekulaardünaamiline simulatsioon elektrolüüdi struktuurile ja ioonjuhtivusele; anoodi, katodi ja elektrolüüdi materjalide molekulaardünaamiline simulatsioon; nanoaku.

Publikatsioone: 4

# *Curriculum vitae*

## **Heiki Kasemägi**

Date and place of birth: November 11, 1974, Tartu, Estonia  
Citizenship: Estonian  
Family status: Single  
Address: Institute of Technology, Tartu University  
Tähe 4 51010 Tartu Estonia  
Phone: +372 5 118754, +372 7 375537  
Fax: +372 7 374 900  
E-mail: cipo@ut.ee

### **Education**

1997–1999 Tartu University, M. Sc. in physics  
1993–1997 Tartu Ülikool, B. Sc. in physics  
1982–1993 Tartu Secondary School No. 7, gold medal

### **Employment**

2003– Institute of Technology, Tartu University, research fellow  
1997–1999 Institute of Experimental Physics and Technology,  
Tartu University, senior engineer  
1997 Institute of Experimental Physics and Technology,  
Tartu University, laboratory assistant

### **Scientific work**

Main fields: materials of **lithium-ion polymer battery** — Molecular dynamics simulation of the effects of inorganic nanoparticles on the structure and ion conductivity of polymer electrolyte; Molecular Dynamics simulation of materials for anode, cathode and electrolyte; nano-battery.

Publications: 4

# DISSERTATIONES PHYSICAE UNIVERSITATIS TARTUENSIS

1. **Andrus Ausmees.** XUV-induced electron emission and electron-phonon interaction in alkali halides. Tartu, 1991.
2. **Heiki Sõnajalg.** Shaping and recalling of light pulses by optical elements based on spectral hole burning. Tartu, 1991.
3. **Sergei Savihhin.** Ultrafast dynamics of F-centers and bound excitons from picosecond spectroscopy data. Tartu, 1991.
4. **Ergo Nõmmiste.** Leelishalogeniidide röntgenelektronemissioon kiiritamisel footonitega energiaga 70–140 eV. Tartu, 1991.
5. **Margus Rätsep.** Spectral gratings and their relaxation in some low-temperature impurity-doped glasses and crystals. Tartu, 1991.
6. **Tõnu Pullerits.** Primary energy transfer in photosynthesis. Model calculations. Tartu, 1991.
7. **Olev Saks.** Attoampri diapsoonis volude mõõtmise füüsikalised alused. Tartu, 1991.
8. **Andres Virro.** AlGaAsSb/GaSb heterostructure injection lasers. Tartu, 1991.
9. **Hans Korge.** Investigation of negative point discharge in pure nitrogen at atmospheric pressure. Tartu, 1992.
10. **Jüri Maksimov.** Nonlinear generation of laser VUV radiation for high-resolution spectroscopy. Tartu, 1992.
11. **Mark Aizengdler.** Photostimulated transformation of aggregate defects and spectral hole burning in a neutron-irradiated sapphire. Tartu, 1992.
12. **Hele Siimon.** Atomic layer molecular beam epitaxy of  $A^2B^6$  compounds described on the basis of kinetic equations model. Tartu, 1992.
13. **Tõnu Reinot.** The kinetics of polariton luminescence, energy transfer and relaxation in anthracene. Tartu, 1992.
14. **Toomas Rõõm.** Paramagnetic  $H^{2-}$  and  $F^+$  centers in CaO crystals: spectra, relaxation and recombination luminescence. Tallinn, 1993.
15. **Erko Jalviste.** Laser spectroscopy of some jet-cooled organic molecules. Tartu, 1993.
16. **Alvo Aabloo.** Studies of crystalline celluloses using potential energy calculations. Tartu, 1994.
17. **Peeter Paris.** Initiation of corona pulses. Tartu, 1994.
18. **Павел Рубин.** Локальные дефектные состояния в  $CuO_2$  плоскостях высокотемпературных сверхпроводников. Тарту, 1994.
19. **Olavi Ollikainen.** Applications of persistent spectral hole burning in ultrafast optical neural networks, time-resolved spectroscopy and holographic interferometry. Tartu, 1996.
20. **Ülo Mets.** Methodological aspects of fluorescence correlation spectroscopy. Tartu, 1996.

21. **Mikhail Danilkin.** Interaction of intrinsic and impurity defects in CaS:Eu luminophors. Tartu, 1997.
22. **Ирина Кудрявцева.** Создание и стабилизация дефектов в кристаллах KBr, KCl, RbCl при облучении ВУФ-радиацией. Тарту, 1997.
23. **Andres Osvet.** Photochromic properties of radiation-induced defects in diamond. Tartu, 1998.
24. **Jüri Örd.** Classical and quantum aspects of geodesic multiplication. Tartu, 1998.
25. **Priit Sarv.** High resolution solid-state NMR studies of zeolites. Tartu, 1998.
26. **Сергей Долгов.** Электронные возбуждения и дефектообразование в некоторых оксидах металлов. Тарту, 1998.
27. **Kaupo Kukli.** Atomic layer deposition of artificially structured dielectric materials. Tartu, 1999.
28. **Ivo Heinmaa.** Nuclear resonance studies of local structure in  $\text{RBa}_2\text{Cu}_3\text{O}_{6+x}$  compounds. Tartu, 1999.
29. **Aleksander Shelkan.** Hole states in  $\text{CuO}_2$  planes of high temperature superconducting materials. Tartu, 1999.
30. **Dmitri Nevedrov.** Nonlinear effects in quantum lattices. Tartu, 1999.
31. **Rein Ruus.** Collapse of 3d (4f) orbitals in 2p (3d) excited configurations and its effect on the x-ray and electron spectra. Tartu, 1999.
32. **Valter Zazubovich.** Local relaxation in incommensurate and glassy solids studied by Spectral Hole Burning. Tartu, 1999.
33. **Indrek Reimand.** Picosecond dynamics of optical excitations in GaAs and other excitonic systems. Tartu, 2000.
34. **Vladimir Babin.** Spectroscopy of exciton states in some halide macro- and nanocrystals. Tartu, 2001.
35. **Toomas Plank.** Positive corona at combined DC and AC voltage. Tartu, 2001.
36. **Kristjan Leiger.** Pressure-induced effects in inhomogeneous spectra of doped solids. Tartu, 2002.
37. **Helle Kaasik.** Nonperturbative theory of multiphonon vibrational relaxation and nonradiative transitions. Tartu, 2002.
38. **Tõnu Laas.** Propagation of waves in curved spacetimes. Tartu, 2002.
39. **Rünno Lõhmus.** Application of novel hybrid methods in SPM studies of nanostructural materials. Tartu, 2002.
40. **Kaido Reivelt.** Optical implementation of propagation-invariant pulsed free-space wave fields. Tartu, 2003.



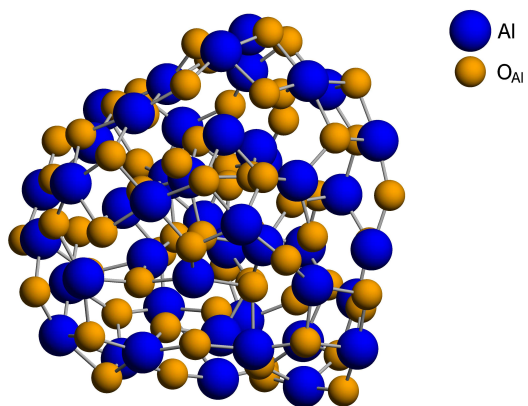


Figure 3.2: A 14 Å diameter “spherical”  $\text{Al}_2\text{O}_3$  particle after “computer annealing” at 2000 K.

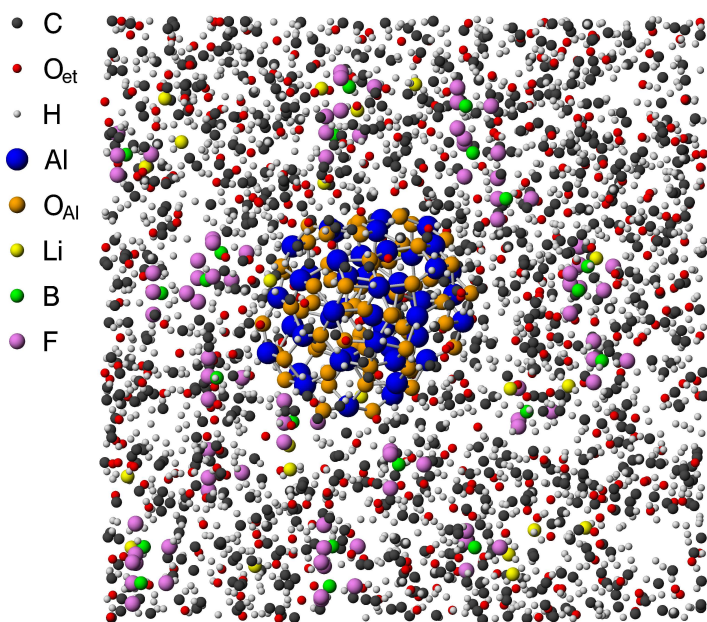


Figure 3.3: A 14 Å diameter  $\text{Al}_2\text{O}_3$  particle in  $\text{LiBF}_4(\text{PEO})_{20}$  before simulation.

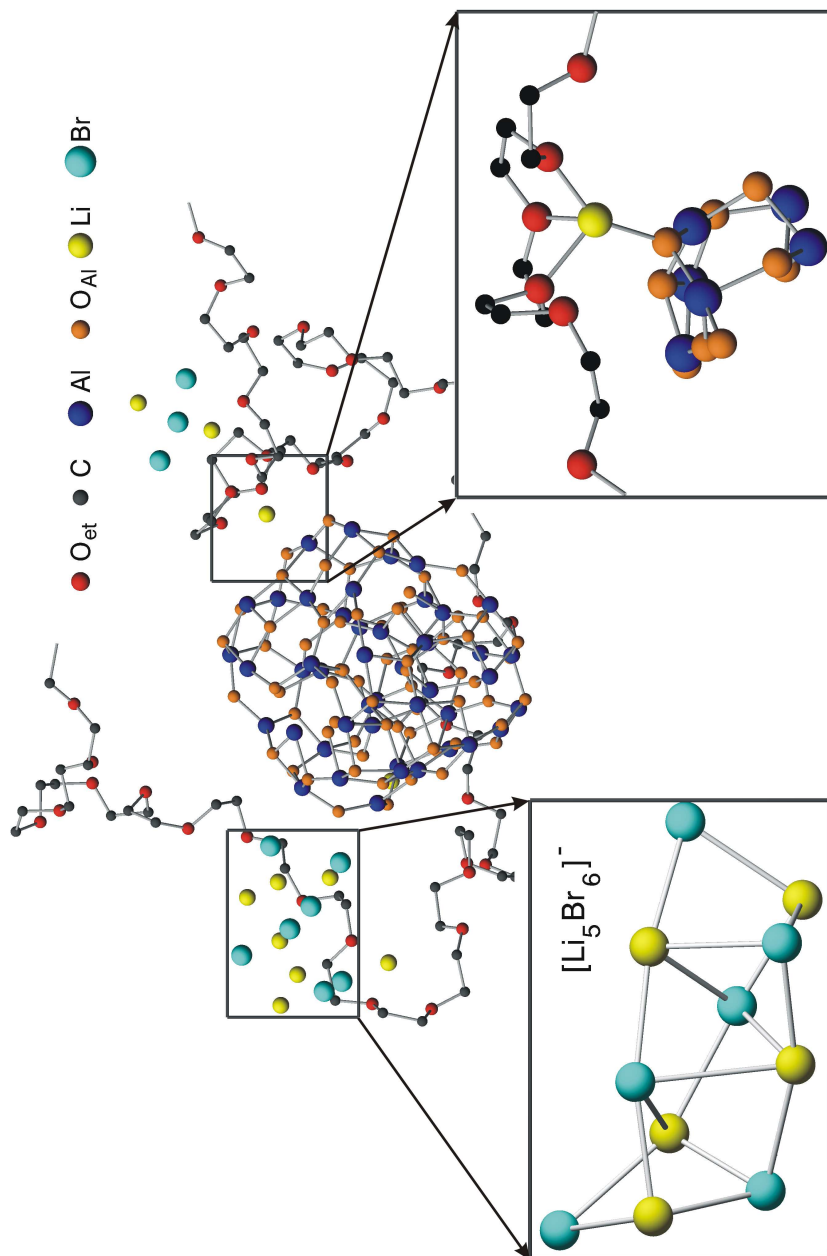


Figure 4.2: A PEO chain around a 14 Å particle in  $\text{LiBr}(\text{PEO})_{10}$  at 360 K, showing the detailed structure around the  $\text{Li}^+$  ion bound to the particle, and an example of an ion cluster.

*Heiki Kasemagi Ph. D. Thesis*



ISSN 1406-0647  
ISBN 9985-56-757-9